THE RHEOLOGY OF SILICON NANOPARTICLE INKS FOR SCREEN PRINTING ELECTRONIC DEVICES

NTOMBIZODWA RUTH MATHE

This thesis is submitted in fulfilment of the requirements for the degree of
Masters in Science in the Department of Physics
University of Cape Town

28 May, 2010

DECLARATION

I know the meaning of plagiarism and declare that all of the work in the document, save for that which is properly acknowledged, is my own.

---------- ----------

Ntombizodwa Ruth Mathe Date

ABSTRACT

In the development of inks for printed electronics, it is important to understand the behaviour of the functional inks and more especially their rheology and surface properties. This project emphasises the importance of ink characterization by performing rheological tests on silicon nanoparticle based inks that are used in the screen printing of electronic devices. The inks were characterized for linear viscoelastic behaviour, flow behaviour, change in properties with angular frequency, as well as thixotropic behaviour. All showed shear thinning, with the more dilute inks showing a power law (Ostwald / de Waele model) behaviour dependence of complex viscosity on angular frequency. The flow behaviour of the inks was also seen to follow a Windhab model. The printability of the inks primarily depends on the shear-dependent viscosity as highly viscous and dilute inks do not produce good printed structures. The printed layers showed electrical and optical activity.

TABLE OF CONTENTS

DECLARATION i

ABSTRACT ii

TABLE OF CONTENTS iii

1. INTRODUCTION 1

2. PRINTED ELECTRONICS 4

2.1. PRINTING METHODS 5

2.1.1. Intaglio printing 5

2.1.2. Planographic printing 6

2.1.3. Relief printing 7

2.1.4. Stencil printing 9

2.1.5. Inkjet printing 10

2.1.6. Printing Inks Requirements 11

2.2. ELECTRONIC DEVICES 12

2.2.1. Printing electronics 13

3. RHEOLOGY 16

3.1. RHEOLOGICAL BEHAVIOUR 16

3.1.1. Viscosity 16

3.1.2. Rheology and rheological properties 19

3.2. COLLOIDS AND THEIR RHEOLOGICAL BEHAVIOUR 24

3.2.1. Formation of colloids 24

3.2.2. Rheology of colloidal systems 26

3.2.3. Printing inks and pastes 28

3.2.4. Rheology of nanoparticle inks 29

3.3. RHEOLOGICAL MODELLING 30

3.3.1. Viscosity model functions 30

3.3.2. Flow curves model functions 31

3.4. SURFACE PROPERTIES OF FLUIDS 34

3.4.1. Surface tension 34

3.4.2. Contact angle 37

4. EXPERIMENTAL PROCEDURE 41

4.1. INK PREPARATION 41

4.2. INK ANALYSIS AND CHARACTERIZATION 44

4.2.1. Rheometry 44

4.2.2. Amplitude sweep 46
4.2.3. Frequency sweep 47
4.2.4. Thixotropy test 47
4.2.5. Contact angle measurements 48
4.3. SCREEN PRINTING OF SILICON NANOPARTICLE LAYERS 50
4.4. PRINTED LAYER CHARACTERIZATION 52
4.4.1. Surface morphology 52
4.4.2. Electrical Characterization 53
5. RESULTS 55
5.1. RHEOLOGY 55
5.1.1. Solvent variation 55
5.1.2. Powder variation 66
5.2. PRINTED SILICON NANOPARTICLE LAYERS 75
5.3. ELECTRICAL CHARACTERIZATION 80
5.3.1. Resistance measurements 80
5.3.2. Photo-response of the printed layers 81
6. DISCUSSION 83
6.1. INK PROPERTIES 83
6.1.1. Rheology 83
6.1.2. Surface Properties of Silicon Nanoparticle Inks 92
6.2. PRINTABILITY 93
6.3. ELECTRICAL CHARACTERIZATION 94
7. CONCLUSION 95
REFERENCES 97
ACKNOWLEDGEMENTS 103

CHAPTER 1: INTRODUCTION

1. INTRODUCTION

This project focuses on the development of silicon nanoparticle inks for printing of electronics, i.e. electronic devices and electronic circuits, on substrates like paper and plastic, using traditional printing methods. Printing of electronics is attractive because it can achieve mass production which can be linked to low costs.

Printing is traditionally used as a means of producing paintings and texts on a substrate, the main objective being the relaying of information. Printing techniques have been used for centuries to develop manuscripts, paintings, books [1]. There are four main categories of printing methods that are used : intaglio, stencil, relief and planar printing [2]. New developments include contactless direct writing methods like inkjet printing. An important factor in printing is the quality of the final image which is dependent on factors like the ink properties, printing methods, type of substrate, etc [3]. Lin, et al, [4] specifically mention that the quality of a print depends on the composition and rheological behaviour of the ink.

Generally, inks contain three main components: a binder (or matrix), a solvent and either a pigment or a dye [3]. In graphic arts and text printing, the pigment and dye are used to give the inks its desired colour and to distinguish the printed layer from the substrate. Pigments are insoluble particles and dyes are miscible solutions, which could either be organic or inorganic. The methods of preparation of the ink are different for different applications and printing methods, as so are the ink requirements. For example, inks for screen printing are more viscous than the inks used for inkjet printing, which are also very dilute.

With the evolution of printing, the technology has improved and is now being used for other purposes like printing electronic devices using functional inks. Printing of electronic devices was started as a way of supplementing some of the components of a circuit [5] and now complete circuits can be produced solely by printing. The study of printed electronics integrates knowledge and developments from printing technology with those from chemistry and materials science, and especially from organic and polymer chemistry [3]. The inks that are used in printing electronics are prepared using organic and inorganic binders, with the active materials being pigments composed of nanoparticles and nanotubes, or as dyes containing conducting polymers, etc. [6]. These inks can be conducting, semiconducting or insulating.

It is important to be able to relate the electrical properties of the printed layer to the rheology of the ink during the printing process. The rheology of the ink is important in any printing application but especially in printing electronics because of the use of functional inks [3]. For example, if the ink has a low viscosity during the screen printing process it will bleed into the substrate, and when the ink is highly viscous it will not print and block the screen mesh. These two extreme cases shows how important it is to understand the rheology of the inks used for printing as these two cases will cause short-circuiting and pin-holes in printed devices [7]. Another important factor in the printability of the ink is its adhesion properties to the substrate. These adhesion and wetting properties can be determined using Young's equation [8] [9], by measuring the contact angle that the ink makes with a solid substrate.

The primary purpose of this investigation is therefore, to develop a relationship between the rheology and wetting properties of the silicon nanoparticle inks, and their dependence on particle loading. A secondary technical aim is to find a single parameter that can be used as a means of predicting the printability of the ink, and to investigate its suitability for characterization of the internal structure and functionality of the printed layer.

The thesis is arranged as follows: literature and background information on printing methods and electronic devices is discussed in Chapter 2. This is followed by Chapter 3 on the rheology and surface science of colloids, focusing on the inks. The experimental procedure is thoroughly explained in Chapter 4, and this is followed by Chapter 5 on the results of the rheology, contact angle, printability of the inks and the electrical characterization of the printed layers. The consolidated results are discussed in Chapter 6, followed by the conclusions based on the results in Chapter 7.

CHAPTER 2: PRINTED ELECTRONICS

2. PRINTED ELECTRONICS

Large-scale printing was created as a means of producing multiple copies of documents, fabrics, papers. Printing techniques have evolved over centuries from woodblock printing, which was first used around AD 200 to modern methods such as inkjet printing and nanolithography [1]. In 1420, intaglio printing was the major printing method that started in Germany [10]. The printing technique that is the focus of this project is screen printing which is a stencil type printing method. This technique was first used by the Japanese and the patent of modern screen printing was first made by Charles Nelson Jones in 1887 , and then in 1907 by Samuel Simon in England [1]. Screen printing involves pushing the ink or paste through a mesh using a squeegee blade at high shear rates [11].

With the evolution of printing methods through the years, applications of these methods have also evolved from printing books, paintings and textiles to electronic devices. The application of graphic art printing techniques to the solution-based patterning of functional materials is considered as a promising standard for manufacturing of large-area, low-cost electronic circuits on flexible substrates. Printed circuits makes changing of circuit design easier than ordinary wiring, especially before production begins [5]. A major goal for the manufacturing of low-cost flexible electronics is the development of solution-based, functional materials that afford both direct printing of electronic components (including resistors, diodes, capacitors, transistors and interconnects) and high performance in devices [12].

2.1. PRINTING METHODS

Traditional printing methods can be divided into four major sections which are intaglio, stencil, relief and planar printing [13]. There are also modern printing methods like inkjet printing, nanolithography, etc. These methods are discussed in detail below with illustrations.

2.1.1. Intaglio printing

Intaglio printing is a process where an image is engraved into the matrix or plate, usually zinc or copper plates. The plate is covered in ink and the excess wiped off, leaving the ink only in the carvings [1]. Then a paper is placed on the plate and compressed with a heavy roller to imprint the image. The three basic types of intaglio are engraving, chemical etching and dry point needle [10]. These describe the manner in which the images are cut into the plates. Figure 2.1 illustrates gravure printing, an intaglio printing process. Intaglio was initially used by metalworkers to print impressions of their work and to record designs [2].

(a)

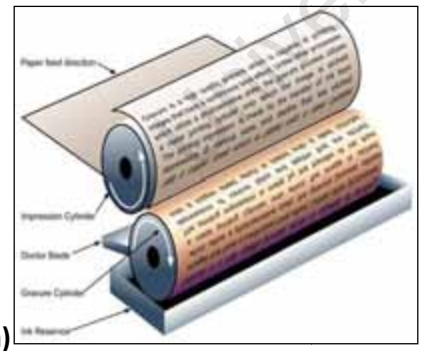

(b)

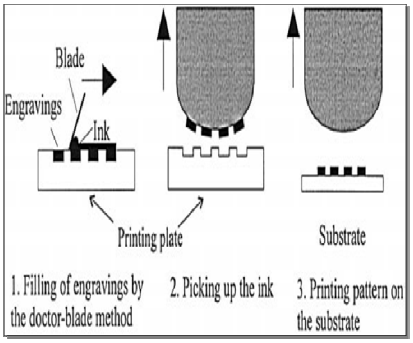

Figure 2.1 (a) An illustration of an intaglio printing process, with the example above of gravure printing. Image obtained from: http://glossary.ippaper.com. Accessed 11/09/09. (b) The image is another illustration of gravure printing [14].

Gravure printing

Gravure printing is an example of intaglio printing [2], and it involves engraving an image onto the image carrier such as copper rollers. The process uses a rotary printing press like flexography and offset printing which will be discussed later. The gravure printing method is mainly used in printing currencies, bank notes, passports and high-value postage stamps. Intaglio printing methods are not commonly used in manufacturing of organic electronics or photonics because of their relative large line widths [15].

2.1.2. Planographic printing

In planographic printing, unlike intaglio, the design to be printed is level with the plate. The main direct planographic printing method is lithography invented by Alois Senefelder in 1798 [1] [2]. In this process, the inked image is transferred (or "offset") from a plate to a rubber blanket, and then to the printing surface [2]. Figure 2.2 is an illustration of an offset planographic printing process. Examples of offset printing are offset lithography and pad printing (offset gravure).

Lithography

Lithography printing is performed using rough surface plates, and oil is used to separate the hydrophobic regions which accept the ink, and hydrophilic regions which reject the ink [16]. The image to be printed is etched onto the plate surface using chemical processes which enable longer and more detailed print runs than the other printing methods like intaglio and letterpress printing [1]. High-volume lithography is used today to produce posters, maps, books, newspapers and packaging.

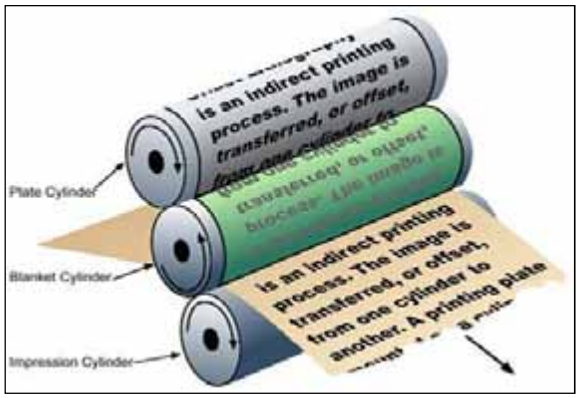

Figure 2.2. The image illustrates the components of an offset printing process. Image is taken from: http://glossary.ippaper.com. Accessed 11/09/09.

The advantages of offset printing are the consistent high image quality, quick and easy production of printing plates and longer plate life, whereas the disadvantage is the slightly inferior image quality compared to gravure printing [1]. Microlithography and nanolithography refers to lithography patterning methods capable of structuring material on a fine scale [17]. Digital lithography is a process that is used to print resist layers, and it was used by Chabinyc et al, to fabricate arrays of hydrogenated amorphous silicon thin film transistors (TFT) [18]. They produced TFTs using a combination of digital lithography to pattern metals and inkjet printing to pattern and deposit a polymeric semiconducting layer.

2.1.3. Relief printing

In relief printing, the image to be transferred onto the substrate is raised above the surface of the printing plate. The ink is applied to the raised surface then rolled or stamped onto the substrate [2]. Printing methods that fall into this category are flexography, letterpress, woodcut, and stamp printing, with flexography being the most common discussed in detail below.

Flexography

Flexography is a printing method that has evolved from letterpress and has been referred to as the updated version of letterpress. This process uses flexible relief plates that can adhere to the printing cylinder, as illustrated in Figure 2.3. The process uses an elastomer plate and a second inking (anilox) roll to achieve uniform coating of the plate cylinder [13]. The substrates that are printed with flexography range from paper to plastic, with final applications in the printing of gift wraps, magazines, retail and shopping bags, food and hygiene bags, self adhesive labels, wall paper, etc.

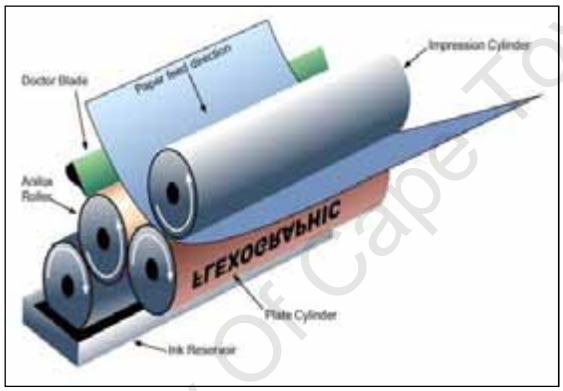

Figure 2.3. The image above is an illustration on a flexography printing process. The image is obtained from: http://glossary.ippaper.com. Accessed 11/09/09.

Flexography has an advantage over lithography in that it can use a wider range of inks, which are water-based rather than oil-based, and is good at printing on a variety of different substrates [1]. The inks used for this printing process are of low viscosity which enables faster drying.

2.1.4. Stencil printing

In stencil printing, the ink is pressed through a flat, thin pattern, [2] , usually with squeegee or blade onto the substrate underneath. Screen printing is an example of stencil printing method.

Screen printing

There are four components of a screen printing machine that are important, as mentioned by a number of authors [3, 19, 20]. They are the screen, substrate, ink and the squeegee to push the ink through the mesh. The screen is made of a finely woven fabric, called the mesh, stretched over a frame of metal or wood [3]. Areas of the screen are blocked off with a non-permeable material to form a stencil, which is a negative of the image to be printed, with open spaces where the ink will be pushed through [2, 21]. Figure 2.4 is an illustration of a screen printing process. The screen is placed on top of a substrate such as paper, fabric or plastic, the ink is placed on top of the screen, and a fill bar (also known as a flood bar) is used to fill the mesh openings with ink [1]. The ink that is in the mesh opening is pumped or squeezed by capillary action to the substrate in a controlled and prescribed amount, i.e. the ink deposit is equal to the thickness of the mesh and or stencil [6].

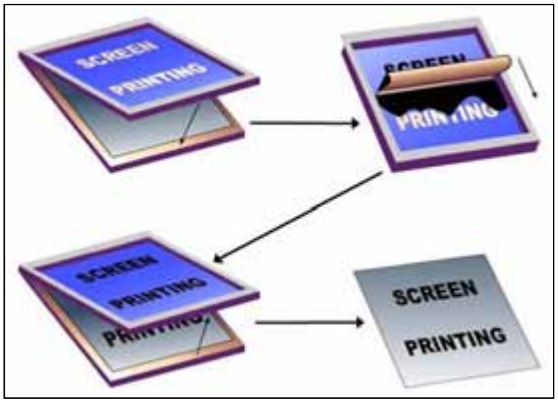

Figure 2.4. The illustration of a screen printing process with the squeegee and the ink. The image was obtained from: http://glossary.ippaper.com . Accessed 11/09/09.

The process of screen printing cycles the ink or paste through low to high shear rates, with a maximum of around 1000 s^{-1}, [4]. This occurs when the paste is pushed through the mesh openings. At different stages of the printing, the ink will be subjected to different shear rates. The impact on the quality of screen-printing pastes should be correlated to their viscosity at high shear rates [3]. Before the paste is screen-printed, the viscosity value for the paste at low shear rates measured using a viscosimeter, is only a reference for determining if there is any change in paste properties and has no direct correlation with printing characteristics [4]. The behaviour of inks at various stages of printing operation can be estimated using rheological measurements, [22], which determines the ink's performance on the press. The fundamentals of rheology and its relation to the printing of inks and paste are further discussed in Chapter 3.

Screen printing is preferred over other processes such as inkjet printing because of its low cost and ability to print on many types of substrates [3]. The advantages of screen printing are low costs, quick turnaround and less smearing [23]. However, the method requires finer powder (low micron to submicron range) and low viscosity pastes, [24], so that the particles do not block the screen.

2.1.5. Inkjet printing

In the inkjet printing process, small droplets of the ink are forced through fine nozzles by pressure pulses created by vibrating piezoelectric crystals [25]. Inkjet methods are based on printing with two types of ink-jet heads, piezoelectric and acoustic types, which are most commonly used for the fabrication of organic electronics [26].

This printing technique can print on various materials, from polymers to metals, at low cost. Due to these advantages, many efforts have been made to use inkjet printing as a manufacturing technique, especially for electronic devices [27]. Compared to other solution phase methods, ink-jet printing holds

greater promise as a means of device integration, as it offers targeted film deposition, and is suitable for industrial-scale production [28]. There has been an increasing focus on printed electronic devices in recent years by means of inkjet printing technology. This is because inkjet printing has significant advantages over conventional lithography technology, i.e. reduction in time, space and waste produced in manufacture [29].

Inkjet printing has been employed in the printing of electronic devices and has over the years gained interest in the solar cell industry as an additive patterning technology [30]. This method of printing has a number of potential benefits, including high material usage efficiency, the avoidance of expensive process steps like etching and vacuum deposition, and the ability to rapidly change circuit designs in real time in a highly cost effective manner [25]. To date, materials like molten metals, conductive polymers, and nano-inks like metal nanoparticles have been printed using inkjet printing. However, high material cost, poor stability and low productivity limit the application of inkjet printing [29].

2.1.6. Printing Inks Requirements

In all these printing methods it is important to control the line and film topology, pin-holing, cracking, and delaminating, and at the same time retain the functionality of the printed layer such as conductivity and capacitance [31]. Another important parameter is the behavior of the inks for each printing method and table 2.1 summarizes the viscosity ranges that are suitable for printing inks, obtained from Pitt [3], Griffiths [1], Fischer [32], and Kippman [33].

Table 2.1. The summary of the viscosity values for printing inks using different printing techniques

Type of ink	Viscosity (Pa.s)	Rheological requirement
Screen printing	3.5 – 5.5	Thixotropic, viscoelastic
Gravure	0.001 – 0.1	Low viscosity inks, viscoelastic
Flexography	0.1 - 5	Slow thixotropic build-up, low yield value
Offset lithography	40 – 100	Highly viscous pastes, thixotropic
Inkjet printing	0.001-0.1	Shear thinning, very low viscosity

Note. The rheological terms used above in describing the inks are discussed in detail in Chapter 3.

Printing has become one of the more affordable methods for mass production of electronics devices, with screen printing and inkjet printing in the forefront. The next section explores electronics and their components as well as touching on the issue of printing electronic devices.

2.2. ELECTRONIC DEVICES

Electronics is a branch of science that refers to the flow of electrons (charge) through non-metallic conductors and semiconductors. An electronic component is any physical entity in an electrical system whose intention is to affect the electrons or their associated fields in a desired manner consistent with the intended function of the electronic system [34]. Electronic components can be classified in various ways, e.g. linear or non-linear; active or passive; two-, three or n-terminal. [35]. Typical examples of electronic systems are capacitors, transistors, resistors, diodes.

A passive device is one which is incapable of augmenting the input power. Examples of passive devices are resistors, inductors and capacitors [34]. An active device is one in which a power gain is possible. These devices do not violate conservation of energy, as they either contain a source of energy such as a battery or are connected electrically to such a source [35]. Examples of active devices are transistors.

Electronics technologies are also classified according to the production methods and assembly. These are discrete electronics, micro electronics, thick film electronics, thin film electronics and printed electronics [13]. Printing electronic devices is the focus of this project and the rest of this section will explore the science of printing electronic devices in detail.

2.2.1. Printing electronics

The principle of printing electronics was known as early as around 1927 with the mass production of printed circuits motivated by the need for producing proximity fuses in mortar shells during World War II [5]. In printing electronic devices, the material being transferred can be either a functional material, such as a semiconductor, or a resist [36]. There have been advances in nanotechnology that have resulted in functional inks used in applications such as flat-panel displays, organic transistors, printed radiofrequency identification (RFID) tags, DNA chips, printed circuit boards, and even 3-D architecture [27]. Different materials have been developed for plastic, flexible electronics including conducting polymers, composites and nanoparticles, which ensure mechanical flexibility together with electronic conduction [37].

The most common methods for printing electronic circuits are spraying, chemical deposition, lithography, screen printing and inkjet printing. Screen printing of electronic circuits has grown over the years because of the process's efficiency of the design, uniformity in mass production, reduction of cost, easier maintenance of parts, and more importantly it provides miniaturization in both circuit printing and components [5]. For devices like conductors, resistors, and dielectrics, screen printing technology began to be widely used during the mid 1960's [24], and has since become the dominant method for thick film deposition. With screen printing, patterning of both inorganic and organic layers is possible. The achievable resolution using this method to too low for printing drain-source contacts (approximately 100 µm), although several groups have reported the fabrication of thin film transistors (TFTs) by screen printing [26].

A printed electrical circuit is produced by printing or forming an electrically conducting pattern on a base or substrate. The printed circuit produces an electrical pattern to which miniature components or parts may be attached as chips or ready-made components; or the circuit may have interconnected elements inseparably associated and formed within a single substrate to perform an electrical function [5]. The circuit is printed onto a rigid or flexible substrate and this could either be thin or thick film. Thick films are produced by such methods as screen printing of inks or pastes, and thin films are generally produced by vacuum deposition [3].

There are different types of circuits such as integrated circuits, monolithic circuits, hybrid circuits, multi-layer printed circuits, and conventional circuit boards. These circuits are produced by different methods such as spraying, photographic and resist, vacuum evaporation, direct and indirect methods. The direct method refers to methods like screen printing [36], whereas indirect production uses several methods to produce the circuit [5]. Printed patterns with incorrect dimensions cannot function at all, and therefore precise realization of a given design is very important for the resulting functionality [27].

There are two general methods for producing integrated circuits; semiconductor and thin-film technology. A semiconductor is a substance whose electrical properties lie between those characteristic of metal and insulators respectively [38]. Printed semiconductor nanomaterials provide new approaches to 3-D heterogeneously integrated system that could be important in various fields of application, including chemical and biological sensors, microeletro-mechanical systems (MEMS), photonics, etc. [39].

Flexible electronic devices currently being used are mainly based on polymeric materials. In 1976, Heeger et al, discovered the conductive abilities of a polyacetylene [40]. The overall performance of an organic electronic device is limited by the conducting properties of the polymer, but some parameters, such as mobility, are not comparable to conventional silicon based devices [37]. The ultimate goal of the broader research, for which this

project is an integral part, is therefore to combine the superior qualities of silicon with the ease of processing organic materials. The main advantage of organic technologies over silicon technologies is the possibility of making low-cost, large area electronics [26]. Among the benefits of organic electronics is the fact that the manufacturing of organic devices may be accomplished partially or entirely by printing. For example, a variety of printing techniques have been employed to define the components of organic thin film transistors (TFT) i.e. gate electrodes, the gate dielectric, the organic semiconductor, and the source/drain contacts [40]. Many existing and emerging electronic devices benefit from the heterogeneous integration of dissimilar classes of semiconductors into single systems, in either 2-D or 3-D layouts [39]. Other types of materials used for printing electronics devices include transparent oxides and nano materials, e.g. carbon nanotubes as the functional part of the inks [37]. Carbon nanotubes are good candidates for flexible electronics because of their flexibility and transparent nature [37].

Because of the importance of the functional inks is producing the devices, the next chapter will deal with the rheological properties of inks. This chapter will explore the different behaviours of printing inks in general and also the surface properties of ink as well as the behaviour of functional inks.

CHAPTER 3: RHEOLOGY

3. RHEOLOGY

3.1. RHEOLOGICAL BEHAVIOUR

Rheology is the study of the flow and deformation behaviour of materials [22, 41]. This area of science focuses on the behaviour of Non-Newtonian fluids under shear stress. Rheology is an important part of many processes and in particular the printing process [3], as discussed in Chapter 2. This chapter will focus on the rheology of materials, define inks as colloids and discuss colloidal systems, and then discuss the rheology of inks and nanoparticle inks. It will also deal with the surface and adhesion properties of inks.

3.1.1. Viscosity

The viscosity of a liquid is the measure of the ratio of the shear stress to shear rate in a fluid [42]. It is commonly perceived as the "thickness" or resistance to flow of the material [43]. Viscosity is the quality that determines the forces that need to be overcome when fluids are used in pipelines, bearings, etc, and which control the flow of fluid in different processes [44]. Viscosity is described as Newtonian when the shearing force per unit area, τ, between two parallel planes of liquid in relative motion is proportional to the velocity gradient, $^{dv}/_{dx}$, between two planes [42]:

$$\tau = \eta \, {}^{dv}/_{dx} \quad , \tag{3.1a}$$

where η is the coefficient of viscosity.

Measurement of viscosity

Maxwell, [45], stated that "the viscosity of a substance is measured by the tangential force on a unit area of either of two horizontal planes at a unit distance apart required to move one plane, the space between being filled with the viscous substance". This concept is illustrated in Figure 3.1, where the movement of the fluid between two parallel plates is shown with the shear stress and velocity gradient.

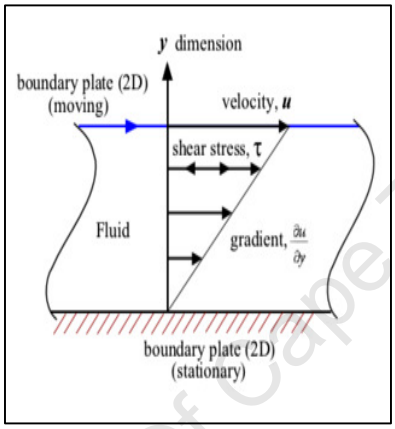

Figure 3.1. Illustration of the forces that act on a liquid during the measurement of viscosity.

There are a number of methods that are used in the measurement of the viscosity of fluids. The two main categories are capillary flow methods and rotational methods, but there are also the falling sphere methods [44]. The capillary flow methods are the most frequently used and measure the viscosity by putting the liquid in a capillary tube under pressure until it starts to flow [45]. This method has advantages in that it is easy to operate and precise. The disadvantage is that the shear rate in the capillary tube varies from the centre to the walls of the tubes, where the shear rate is at a maximum [42].

The rotational methods use a concentric cylinder and a cone-and-plate instrument to measure the viscosity of a fluid [22]. Rotational viscosimeters are useful for the study of non-Newtonian flow behaviour, [43], because they permit the velocity gradient to be kept constant throughout the sample.

Weissenberg developed a cone-plate rheometer that measured both tangential and normal forces in rotation and oscillation [42]. This type of rheometer produces information about the behavior of a material under increasing shear stress, rather than for a single viscosity value [22], as well as other rheological properties such as the storage and loss modulus to be discussed in section 3.1.2.

Newtonian and non-Newtonian fluids

Newtonian fluids are defined as fluids where the shear stress, τ, is directly proportional to the rate of shear, $\dot{\gamma}$, [44]. The constant of proportionality, η, is known as the viscosity coefficient or viscosity. Equation 3.1a can thus be rewritten as:

$$\tau = \eta . \dot{\gamma} \ , \qquad (3.1\ b)$$

For a Newtonian fluid, the shear viscosity is independent of the degree or duration of the shear load [22]. This means that regardless of the force acting on a fluid, it continues to flow steadily. A plot of shear stress against strain rate for Newtonian fluids will be linear as shown in Figure 3.2. Common examples of such fluids are single phase liquids like water, solvents, some pure polymers and mineral oils.

Non-Newtonian fluids are fluids whose properties change with the applied load and whose flow cannot be described by a single constant viscosity [44]. Non-Newtonain fluids will therefore have a non-linear shear stress and strain rate relationship, see Fig.3.2, which can be described by a power law index model, [46]:

$$\tau = K \dot{\gamma}^{n} \ , \qquad (3.2)$$

where, τ, is the shear stress; $\dot{\gamma}$ is the shear rate, K is the consistence index and n, is the power law flow index. For shear thinning fluids, $0 < n < 1$, and the more shear thinning the material, the closer it is to zero [43, 46].

Shaw [42] explained the main causes of non-Newtonian flow as the formation of a structure throughout the system and the orientation of asymmetric particles in the fluid caused by the velocity gradient. Common examples of non-Newtonian fluids are paint, starch, polymer solutions and inks.

Figure 3.2 illustrates the flow behaviour for Newtonian and non-Newtonian fluids under increasing shear rate. The dilatant and pseudoplastic fluids represent non-Newtonian behaviour.

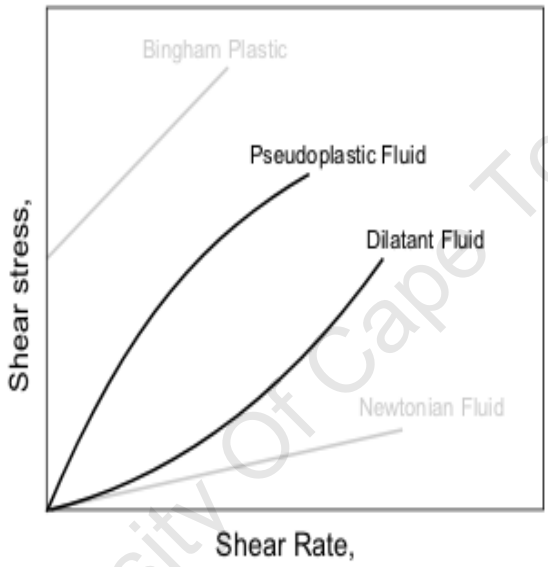

Figure 3.2. Shear rate vs. shear stress curves for Newtonian and non-Newtonian fluids. This shows the different behavior of fluids under shear stress [42].

3.1.2. Rheology and rheological properties

Rheology is a branch of science that focuses on the flow and deformation of materials [44]. This is a sub-discipline of fluid dynamics that deals with the flow behaviour of non-Newtonian fluids, as illustrated by the table 3.1. Fluid mechanics incorporates both Newtonian and non-Newtonian fluids and their rheology. The behaviour of non-Newtonian fluids is intermediate between the Hookean elastic solids and Newtonian viscous fluids [42]. This intermediate behaviour is called viscoelastic as the materials posses both viscous and elastic characteristics depending on the amount of shear loading [22].

Table 3.1. The table to show the relation of rheology in regards to fluid mechanics. Taken from www.answers.com/topic/rheology. Accessed 27/06/09.

<table>
<tr><td rowspan="4">Continuum mechanics</td><td rowspan="2">Solid mechanics or strength of materials</td><td colspan="2">Elasticity</td></tr>
<tr><td>Plasticity</td><td rowspan="3">RHEOLOGY</td></tr>
<tr><td rowspan="2">Fluid mechanics</td><td>Non-Newtonian fluids</td></tr>
<tr><td colspan="2">Newtonian fluids</td></tr>
</table>

There are two important steps in the rheological characterization of a material. The first it is to determine the appropriate rheological test apparatus, and the second is to determine the appropriate test for measuring rheological properties relevant to the intended application of the material [7]. Based on this, the properties that define the rheology of a material which are the viscosity, storage modulus, loss modulus, shear stress, shear rate, strain percentage, and angular frequency can be defined [22, 42, 44].

- Complex viscosity (η^*) is a frequency-dependent viscosity function determined during the harmonic oscillatory shear. The complex viscosity function is equal to the difference between the dynamic viscosity (real part) and the imaginary part of the complex viscosity:
  $\eta^*(\omega i) = \eta'(\omega) - i\eta''(\omega)$, (3.3)
  where η^*, is the complex viscosity, η' is the real part of the complex viscosity representing the viscous behaviour and η'' is the imaginary part of the complex viscosity representing elastic behaviour of the material.

- Shear stress (τ) is the tangential component of the force per unit area acting on the surface on any surface in the fluid and is given by equation :
  $\tau = {}^{F}/_{A}$, (3.4)
  where F is the shearing force and A is the shearing area. (see Figure 3.3a).

- Storage modulus (G') is the measure of the deformation energy stored in the sample during the shearing process, and it represents the elastic behaviour of the sample.

- Loss modulus (G'') is the measure of the deformation energy lost by the sample during the shearing process, and it represents the viscous behaviour of the sample.

The relationship between the storage and the loss modulus is defined by the loss factor (or damping factor), δ, as:

$$\tan\delta = {}^{G''}/_{G'} \qquad (3.5)$$

The loss factor is the ratio of the viscous to the elastic portion of the deformation behaviour [22]. The tack behaviour or tackiness (length of the materials during application) of a material can be determined by controlling the loss factor.

The above properties are determined using forced-oscillation measurements. These are destructive methods that are used to determine the viscous and elastic behaviour of materials [47]. The independent parameters in such rheological measurements are the shear rate, strain percentage and the angular frequency. Definitions are obtained from [22, 42, 44]:

- Strain is a dimensionless unit that is described as the change in angle between line elements initially orthogonal to each other. It is given by the following equation:

$$\gamma = {}^{s}/_{h}\,, \qquad (3.6)$$

where s is the deflection and h is the distance between the measuring plate, i.e. gap dimension, as illustrated in Figure 3.3b:

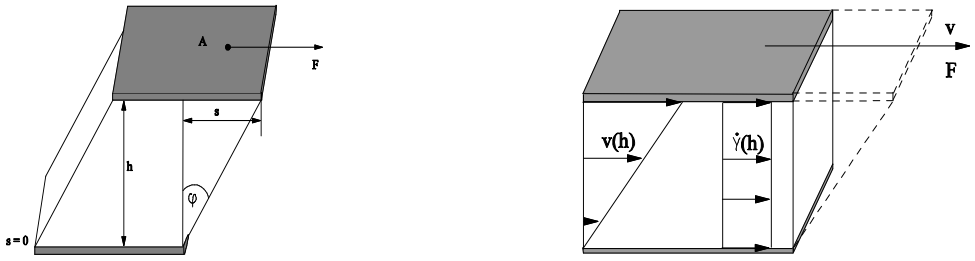

(a) (b)

Figure 3.3. Illustration of the shear stress and shear rate of a fluid between two measuring plates [48].

- Shear rate is the time-dependent rate of deformation. It has synonyms like shear gradient, velocity gradient, strain rate and deformation rate, and is defined as:

$$\dot{\gamma} = {}^{v}/_{h}\,, \tag{3.7}$$

where v is the velocity in m/s and h is the gap between the measuring plates in metres.

- Angular frequency (ω) is defined by the number of oscillations per unit time in oscillation tests. In rheology, as in most areas of physics, angular frequency is more widely used than linear frequency.

During steady shear flow, the strain rate dependence of the additional viscous stress reflects the interplay of dissipative mechanisms, like fluid flow and droplet rearrangements, with storage mechanisms like deformation [49]. Rheological behaviour can be used to predict the nature of a suspension. For example, in gels, the elastic modulus characteristically dominates the viscous modulus at low frequencies [50].

Fluids can therefore be defined by their rheological behaviour, [4], which will also determine how the material will behave in end-use environment [50]. The definitions of rheological behaviours below were taken from discussions of rheology by Shaw and Mezger [22, 42].

- Shear thinning materials show a decrease in viscosity when put under increasing shear rate, e.g., polymer solutions, paints and inks.
- Shear thickening (dilatant) materials are the type of materials whose viscosity increases as the strain on the material increases, e.g., ceramic suspensions, starch dispersions (with high particle loading).
- Thixotropic behaviour is the characteristic of the material where the material recovers after being put under high shear rates and then back to rest. The structural strength during the shear loading phase decreases but there is complete structural regeneration during the rest period. This process can be reversible or irreversible and it is a time-dependent analysis.
- Rheopectic behaviour is the opposite of thixotropy where there is an increase in the structural strength during decomposition and complete regeneration at the rest phase.

3.2. COLLOIDS AND THEIR RHEOLOGICAL BEHAVIOUR

Colloids are systems in which there exist two phases: the continuous phase or matrix and the dispersed phase, with one of the phases having dimensions that are within the micrometers to nanometres range in size [42]. The dispersed phase is normally small (the particle sizes of the dispersed phase in a colloidal system range from 1 nm to 1 µm), in order to have negligible gravitational forces and for the interactions to be dominated by short-range forces, such as the Van der Waals and surface charge [51]. Colloidal solutions show a behaviour that is intermediate between Hookean and Newtonian behaviour [52], presenting both the elastic and viscous characteristics.

Colloidal dispersions often show distinctive behaviour that deviates from Newtonian behaviour, and for example behaving as solids until a finite amount of stress is applied, at which point they yield before deforming continuously like liquids [53]. An important characteristic of the colloidal state is that the colloidal particles must be large enough to give a characteristic slow rate of diffusion, and sufficiently small to remain suspended indefinitely in the liquid medium [52]. In other words, the particles in a colloidal dispersion, though small, must be large enough to have a definite surface separation between the particles and the matrix [54]. The particle sizes as well their shape, is important in determining the properties of a colloidal system [42].

3.2.1. Formation of colloids

The formation of a colloidal solutions depends of a number of factors like the particle size, shape and flexibility, surface properties, particle-particle interactions and the particle-solvent interactions [42]. All these parameter have to be taken into consideration when preparing a colloidal suspension and especially for the stability of the colloid. There are different methods of stabilising a colloidal system, with the two main categories being electrostatic and polymeric stabilization. An unstable colloid occurs when the repulsive

force is not strong enough to balance the attractive van der Waals force between the particles, resulting in clusters that precipitate out of solution [42].

Table 3.2, updated from Burton's table [42, 52], is a general illustration of the phases that are present in a colloid and the different types of colloids that are formed based on the starting material.

Table 3.2. The formation of different types of colloids depending on the starting material.

	Dispersed phase	**Dispersion medium**	**Colloids name**	**Examples**
1	Solid	Solid	Solid suspension	Pigmented plastics, porcelain, paper
2	Liquid	Solid	Solid Emulsion	Cheese, butter
3	Gas	Solid	Solid foam	Plaster, metallic foams
4	**Solid**	**Liquid**	**Sol, colloidal suspension, pastes**	**Gelatine, starch solution, inks, toothpaste**
5	**Liquid**	**Liquid**	**Emulsion**	**Inks, milk, mayonnaise**
6	Gas	Liquid	Foam	Whipped cream, fire extinguisher foam
7	Solid	Gas	Solid Aerosol	Dust, industrial smoke
8	Liquid	Gas	Liquid Aerosol	Liquid sprays, fog

The highlighted colloidal formations, in table 3.2, are of main interest in this project and can be further divided into sections as determined by Ostwald and later by Graham [52].

3.2.2. Rheology of colloidal systems

As discussed in Chapter 2, the rheology of inks is an important characteristic in the measure of the ink's printability, adhesion properties and general behaviour under increasing shear load. Rheological measurements of colloids are of great importance because they can furnish quantitative information regarding the structure of the colloidal suspension and hence specific particle interactions [55]. The rheological behaviour of colloidal dispersions depends on factors such as the viscosity, particle concentration, particles shape and size, and the particle-particle interactions [42, 56]. Colloidal systems in media of intermediate polarity are important industrially, for example in the ink, paint industries, although there is little reported work on the rheology of such systems [57]. This is because the rheological behaviour is complex due to the colloidal system's thermodynamically non-ideal characteristics. However, generally they do not show substantial elastic recovery characteristics like polymeric fluids [53].

Knowledge of the rheological properties of suspensions is important because they control the flow behaviour as well as the viscosity and the elasticity of the suspension [58]. Different authors have worked on the rheology of colloidal systems and of these, Mewis [59], observed that when a fluid is systematically added to a dry powder, the system passes through several transition stages of colloid formation. The rheological behaviour of colloidal dispersion varies from a low-viscosity fluid to a highly elastic paste, depending on the particle volume fraction and the interaction forces between the particles [60]. Most colloids show viscoelastic behaviour, which is described by the energy storage and / or dissipation of the material under shear stress. This results in the material having either elastic or plastic behaviour depending on whether the energy is stored or dissipated [42]. The viscoelastic properties of stable colloidal systems comes from the repulsive interparticle potential [24]. The viscoelastic properties become more significant when the particle concentration is increased. Many concentrated suspensions display a pasty behaviour above critical concentration, when under low mechanical strains

they behave almost as viscoelastic solids, whereas under high stresses they flow like a viscous liquid [61]. The viscoelastic response should be taken into consideration because it can provide more detailed information about the structural conditions of the disperse phase in the equilibrium. The knowledge of viscoelastic properties enables one to define the most suitable composition of the colloidal suspensions [24].

For the rheology of colloidal systems, more emphasis is placed on the linear viscoelastic properties and the time dependence of the colloids at low strains. This is because of the presence of the short range intermolecular forces which prevents the colloid from having a recovery mechanism after high strains [54]. Lin et al, [4], used viscosity curves to show that most printing pastes show shear thinning behaviour, indicating the presence of weakly attractive network. It is widely believed that shear thinning is due to ordering of the particles into layers or strings which reduce the energy dissipated under shear [62]. It has also been postulated that the shear thinning is due to a distortion of the liquid-like structure which presumably leads to a decrease in energy dissipation [63].

The increase in viscosity with shear rate observed for shear thickening systems is normally accounted for by a change in the system from an ordered to disordered state [24]. Hoffman has reviewed the explanations for shear thickening and he was also the first to offer evidence of a change from an ordered to a disordered state when thickening occurs [57], which was also observed by Zupancic et al, [24], using rutile suspension in epoxide and acrylic resin . This is in disagreement with D'Haene et.al, [64], who account shear thickening to the generation of particle clusters and not the destruction of ordered layers.

3.2.3. Printing inks and pastes

The rheology of inks has been extensively studied over the years [65]. For printing inks it is important to determine the full rhelology because the viscosity of an ink at low shear rates tested using a viscosimeter has no direct correlation with other paste properties such as, printing characteristics, which are performed at high shear rate [4]. The rheology of thick film inks is controlled by the viscosity of the ink and the surface tension of the ink and their dependence on shear rate and time [3]. Both of these properties are related to the inter-atomic forces within the body of the fluid, viscosity being regarded as the resistance to motion of one layer of fluid over another, while the surface tension arise from the imbalance of forces at an interface between two different materials [3].

Printing inks are viscoelastic substances and they show time-dependent elastic and viscous behaviour under shear stress. The printability of an ink depends on its viscoelastic behaviour, its rheology and therefore attention should be given to the study of the inks, their binder, solvent and as a paste/mixture [47]. Additives in the printing paste control the rheology of the paste during printing and are used to install thixotropic behaviour [66]. In the formulation of inks for electronic materials, solvents with different evaporation rates control the evaporation behaviour and rheology, avoiding the use of other additives as much as possible [67].

There are different behaviours of the ink during the print process and the thixotropy becomes the predominant parameter after the ink has been pushed through the mesh, whereas the viscoelastic properties have an effect when the flexible meshes return in position after deformation and there is the detachment of the ink on the screen [6]. When printing using screen printing, to have good screen printing performance the particle suspension must be thixotropic to avoid pinholes [7]. The interaction between the ink and paper substrate after printing is evaluated by using the measurement of the ink mileage and transfer curves on paper [68].

3.2.4. Rheology of nanoparticle inks

The use of nanoparticles in functional printing pastes is motivated by the fact that nanoparticles already have all the required electrical and optical properties and can be used as simple building blocks to form complex structures at a small scale [67]. The rheology of nanoparticles refers to the pastes that are prepared by suspending nanoparticles in an organic binder medium, forming a colloidal system. The increased specific surface area and the surface characteristics in nanoparticles, contributes to the difficulties in obtaining stable nanoparticle dispersions, as compared to micrometer-sized particles [69]. The nanoparticles are susceptible to agglomeration more than the micron-sized particle, due to high specific surface area of the nanopowders.

The Van der Waals forces present in the aggregation of nanoparticles are attractive, and the repulsive are forces between the molecules. For most colloidal forming processes, a suspension with high solid loading level (>50%) is desirable [63]. The powdered suspensions of nanoparticles in a shear-thinning regime tend to become a two dimensional, layered arrangement as shear rate increases to infinity, which results in a structural evolution in the suspension as a function of shear rate [69].

For inks with electrical properties the control of the rheology is more difficult than the simple pigment colour inks [67]. Ogawa, et al, theorized that the viscosity increase with a decrease in particle size, is due to the increase in the overlapping area of the electrical double layer around each particle, which agrees with experimental data [63]. And in [69], the dispersion qualities of the inks were examined by rheological characterization.

3.3. RHEOLOGICAL MODELLING

Mathematical modeling functions for curve approximation are used to describe the complete flow or viscosity curve using a small number of curve parameters. The most often used rheological models are separated into viscosity and flow curve model functions [22].

3.3.1. Viscosity model functions

The viscosity models are model functions that do not have a yield point, i.e no initial stress is required in order for the material to start flowing. The general requirement for the viscosity model is that the viscosity should decrease with an increasing shear rate [70]. The simplest is a power law model of the viscosity function, first attempted in 1929 by Ostwald / de Waele [71]. In this model, the viscosity is given by:

$$\eta = K\dot{\gamma}^{n}, \tag{3.8}$$

where η is the viscosity, $\dot{\gamma}$ is the shear rate, K is a constant, and n is the power law index [70, 71]. The power law index describes whether the material is shear thinning or shear thickening. For shear thinning materials, $0<n<1$ and for shear thickening materials $1<n<\infty$ [4, 22, 72]. The complex viscosity as a function of angular frequency can be used by converting the shear rate to angular frequency using the Cox-Merz rule [71], i.e. $\eta(\dot{\gamma}) \equiv |\eta^{*}(\omega)|$ for $\dot{\gamma} = \omega$.

Taking the natural logarithms of both sides of equation 3.8 result in the equation: $\ln(\eta) = (n)\ln(\dot{\gamma}) + \ln(K)$ and a plot of $\ln(\eta)$ against $\ln(\dot{\gamma})$ shows a linear relationship [70]. It is also quite easy to fit experimental data this model and determine the constants K and n. Because this model is only suitable for lower shear rates, it needs to be modified to include higher shear rates. The modified model functions are designed for unlinked polymers and are not suitable for dispersions and gels [22]. Examples of the modified model functions are the Cross and Carreau model.

The Cross model describes the viscosity as:

$$\eta = \frac{\eta_0}{1+(\frac{\eta_0 \dot{\gamma}}{\tau^*})^{1-n}} \quad , \tag{3.9}$$

where τ^* is the shear stress at the transition between Newtonian and power law behaviour, $\dot{\gamma}$ is the shear rate and η_0 is the zero-shear viscosity.

In the Carreau model, the viscosity is given by:

$$\frac{\eta-\eta_\infty}{\eta_0-\eta_\infty} = [1 + (\lambda\dot{\gamma})^2]^{\frac{(n-1)}{2}} \quad , \tag{3.10}$$

where η_∞ is the viscosity at infinite shear rate, η_0 is the viscosity at zero shear rate, $\dot{\gamma}$ is the shear rate n is a constant and λ is a time constant.

3.3.2. Flow curves model functions

Different rheological models exist that describe viscous flow functions of the fluid system, i.e. the systems with a yield stress [73]. These models, which approximate real flow behaviour, include the Casson, Windhab, Bingham models and are listed in table 3.3 [73].

Table 3.3. The model functions for plastic and viscous flow of fluids.

Rheological model	Equation
Bingham	$\tau = \tau_0 + \eta.\dot{\gamma}$
Casson	$\tau^{1/2} = \tau_0^{1/2} + (\eta.\dot{\gamma})^{1/2}$
Heinz	$\tau^{2/3} = \tau_0^{2/3} + (\eta.\dot{\gamma})^{2/3}$
Casson (general)	$\tau^{1/n} = \tau_0^{1/n} + (\eta.\dot{\gamma})^{1/n}$
Herschel-Bulkley	$\tau = \tau_0 + K\dot{\gamma}^n$
Schulman-Haroske-Reher	$\tau^{1/n} = \tau_0^{1/n} + (K\dot{\gamma})^{1/m}$
Tscheuschner	$\tau = \tau_0 + \eta_\infty.\dot{\gamma} + \eta_{strl}.{}^{\dot{\gamma}}/_{\dot{\gamma}_r^n}$
Windhab	$\tau = \tau_0 + \eta_\infty.\dot{\gamma} + (\tau_1 - \tau_0).[1 - \exp(-\dot{\gamma}/\dot{\gamma}^*)]$

In table 3.3, τ = shear stress, τ_0= yield stress, τ_1= maximum shear-induced stress, η = viscosity, $\dot{\gamma}$ = strain rate (shear rate), η_∞= final viscosity and $K, n, m, \dot{\gamma}^*$ are constants.

For very small yield stress,τ_0, the Bingham, Casson and Heinz models all transform into a description of the basic Newtonian viscosity. The yield stress is determined by curve fit or by extrapolation and there is generally a good agreement between the raw data and the models at high shear rates [73]. Zupancic et al, successfully used the generalized Casson model for describing plastic flow of colloidal suspensions [24].

The Windhab model was first used to describe the flow behaviour of molten chocolate by assuming that when the molten chocolate is put under shear, there is a change in the internal structure [22]. The rheological description of the model is based on measurable physical parameters, which affect the flow/textural characteristics in 'structured' multi-phase system [22, 73]. Many flow functions of concentrated fluid systems can generally be described by a superposition of a measured yield value (τ_0), to a flow function in the high shear region (η_∞), and an intermediate flow function region, $\eta(\dot{\gamma})(\tau_1)$, which describes the flow curve when the inner structure changes from the isotropic state of rest structure, characterized by τ_0 to a shear induced structure [73]. The Windhab model flow behaviour is characterized by the strain rate and shear stress relationship in Figure 3.4. τ_1 is the shear-structuring limit determined by linearly extrapolating the flow function from the high shear domain to the τ-axis.

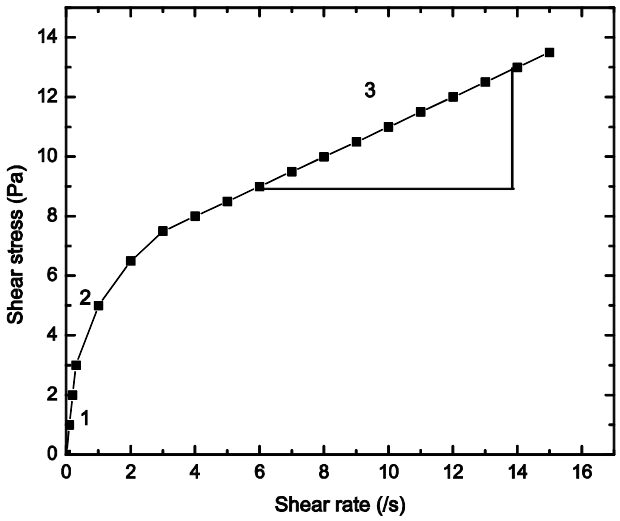

Figure 3.4. The flow curve according to Windhab model [22].

The three regions identified in Figure 3.4 represent the different structural changes that the material undergoes during shear: 1 represents the measured yield value; 2 represents the intermediate flow region which describes the shear induced structure; and 3 represents the flow function in the high shear region, which is similar to the flow of pure Newtonian fluids [73].

In physical terms the shear-induced structuring is caused by a combination of mechanisms, e.g. particle orientation, or forming of micro-layers in systems like chocolates, starch suspensions, and $CaCO_3$ suspensions [74]. Shear stress change during the shear induced structuring region can be described with an exponential function between shear stresses τ_1 and τ_0, which depends on the solid volume fraction, particle size-distribution and particle-particle interactions. The constant $\dot{\gamma}^*$ can be calculated from τ_1 and τ_0. In order to find the point of the curve where the final viscosity, η_∞, is reached, the Windhab model has a second parameter $\tau^* = \tau(\dot{\gamma}^*)$ indicating that the shear-induced loss of structure is at a maximum when $\dot{\gamma} = \dot{\gamma}^*$ is reached [73, 74].

3.4. SURFACE PROPERTIES OF FLUIDS

3.4.1. Surface tension

Shaw, [42], defines the surface tension of a liquid as the force acting at right angles to any line of unit length on the liquid surface. The surface tension and surface free energy can also be defined as the work required to increase the area of a surface isothermally and reversibly by a unit amount. de Gennes defines the surface tension of a fluid as an effect within the surface layer of a liquid that causes the layer to behave as an elastic sheet [75]. This results in the molecules on the surface of a liquid behaving differently from the bulk molecules. Surface tension is not a property of the liquid alone, but a property of the liquid interface with another medium. Figure 3.5 shows the different forces acting on the molecules of the fluid in equilibrium.

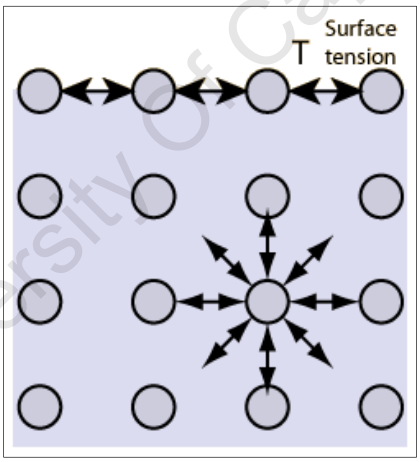

Figure 3.5. An illustration of the forces acting on the bulk and surface molecules of a liquid.

The short-range intermolecular forces that are responsible for the surface / interfacial tensions are the Van der Waals forces (the London dispersion forces) and hydrogen bonding (e.g. in water) and metal bonding (e.g. mercury) [42].

Surface tension measurements can be performed by means of a number of different commercially available techniques like the tensiometer, drop-shape analyzer, etc, [76]. The Wilhelmy plate (WP) and du Noüy ring are invasive measurements while the maximum bubble pressure and oscillation jet are non-invasive [42]. The WP method is one of the oldest and most direct measurements of surface tension.

The dynamic surface tension, γ_{dyn}, plays an important role in many physical processes including wetting and two plate flow [77]. Wetting is the displacement from the surface of one fluid by another and the different types of wetting are spreading, adhesional and immersional wetting [42]. The surface energy is an important property that influences the wettability and the layer-by-layer deposition of thin films [9]. Surface energies are estimated using the theory of the adhesion work among solid and liquid phases, where polar and non-polar (dispersive) contributions in the interaction process are considered, using two liquids with different polarity, e.g. water, γ =72.80 mN/m and glycerol, γ =64.0 mN/m. Fowkes approach is used by Vladuta in describing wetting and adhesion process in conjunction with contact angles for many systems [9].

Surface energy depends on the chemical structure of the solid and wettability depends on the surface morphology and on the contact liquid [9]. For solid-liquid systems, surface tension is defined by the wetting of a liquid onto a solid substrate and the free energies of the wetting methods are given by the following equations [42]:

Spreading wetting

$$-\Delta G/A = S = \gamma_{SV} - \gamma_{SL} - \gamma_{LV} \quad (3.11)$$

Adhesional wetting

$$-\Delta G/A = Wa = \gamma_{SV} - \gamma_{SL} + \gamma_{LV} \quad (3.12)$$

Immersional wetting

$$-\Delta G/A = \gamma_{SV} - \gamma_{SL} = \gamma_{LV} cos\theta \quad (3.13)$$

From the spreading wetting equation:

$$\Delta G/A = S = \gamma_{SL} + \gamma_{LV} - \gamma_{SV} \quad (3.14)$$

$$dG = \gamma_{SL} dA + \gamma_{LV} cos\theta - \gamma_{SV} dA \quad (3.15)$$

At equilibrium, $dG = 0$

Therefore it gives Young's equation [8] which is:

$$\gamma_{SL} + \gamma_{LV} cos\theta - \gamma_{SV} = 0 \quad (3.16)$$

where ΔG is the free energy due to spreading, S is the spreading coefficient and Wa is the work (free energy) of adhesion.

For a flat smooth surface, the contact angle θ is defined by the equilibrium condition of three interfacial tensions: solid-liquid, γ_{SL}, solid-vapour, $\gamma_{SV}$and liquid-vapour, γ_{LV} which are related through the Young's equation [8].

Equation 3.16 can be written in terms of surface tension to give the Young's equation:

$$\gamma_S = \gamma_{SL} + \gamma_{LV} cos\theta \quad (3.17)$$

Note: $\gamma_{SV} = \gamma_S$

To use Young's equation without correction for roughness and chemical heterogeneity, only very smooth and homogeneous films have to be chosen the for determination of the γ_S, [78].

3.4.2. Contact angle

When a liquid is dropped onto a solid substrate, all the forces are balanced. At the point of the liquid-solid contact they form a contact angle, θ, which is the angle that the tangent to the surface of the droplet makes with the solid substrate [75]. The contact angle is a surface property and is a result of the intermolecular interactions within the liquid and with the solid substrate [9], see Figure 3.6.

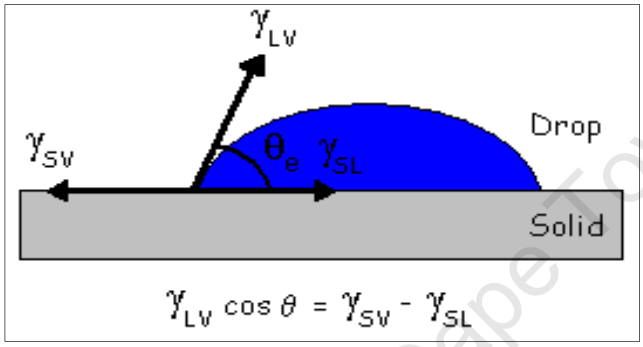

Figure 3.6. The image of the contact angle of a liquid droplet on to a solid surface and the forces acting on the droplet. The three forces acting on the droplet are in equilibrium.

The measurement and determination of contact angle for solid substrates is important in formulating products like adhesives, and in understanding solid-solid and solid-liquid intermolecular interactions. Tavana, et.al, pointed out that the relationship between contact angle and surface tension cannot be obtained by the method of simply placing a droplet of the liquid onto the solid substrate and measuring the static contact angle using a goniometer [79]. When a liquid makes contact with a solid substrate and adheres to it, the area of liquid-gas interface decreases, which is in contrast to spreading wetting, where the solid-liquid interface increases [42]. To determine the surface tension of a fluid, equation 3.9 has been derived into Young's equation, 3.16. This then is used to assess the surface tension / energy, $\gamma_{SV,}$ using the contact angle measurements [80]:

$$\gamma_{SV} = \gamma_{SL} + \gamma_{LV} cos\theta \qquad (3.16)$$

Because the interest lies in the solid-liquid interface, the effect of the solid vapor interface can be written as just the solid surface tension, as therefore the equation will be:

$$\gamma_S = \gamma_{SL} + \gamma_{LV} cos\theta \qquad (3.17)$$

Equation 3.17 is for ideal smooth, rigid, chemically homogeneous, insoluble and non-reactive surfaces [78]. This equation, 3.17, can be used to calculate γ_S, if γ_{SL} can be predicted from additional information for ideal surfaces.

Surface characterization is important in many fields of science and contact angle measurements are used extensively for this purpose [9]. An advantage of contact angle measurements is that the method can be used in a non-destructive manner [81]. The Zisman plot, Figure 3.7, is used to estimate the surface tension of the solid surface based on contact angle measurements [42]. This is a plot of the cosine of contact angle of a series of liquids as a function of the liquid surface tension of a know solid surface [79].

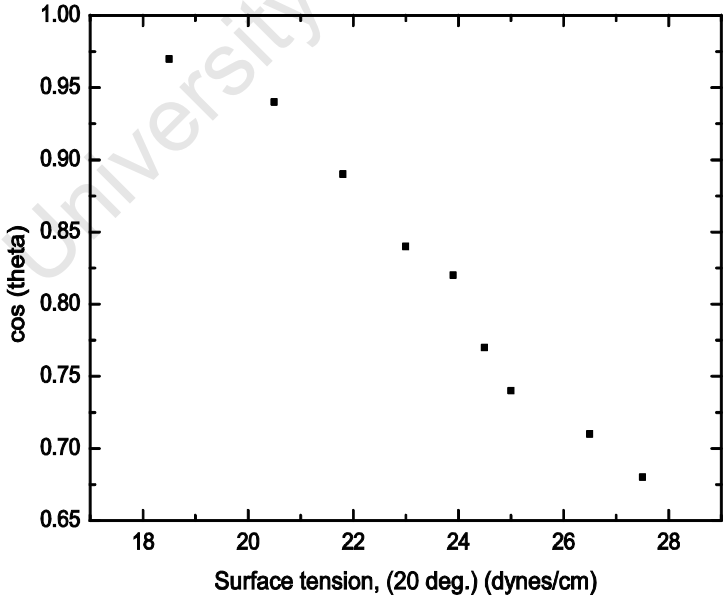

Figure 3.7. The Zisman plot for the determination of surface tension of liquids based on the contact angle measurements, the above figure is a plot for n-alkanes [75, 80].

If we apply the Fowke's semi-empirical interfacial tension to the solid-liquid interfaces, then:

$$\gamma_{SL} = \gamma_S + \gamma_{LV} - 2(\gamma_S^d . \gamma_{LV}^d)^{1/2} \ . \quad (3.18)$$

Combined with Young's equation (equation 3.16), this becomes:

$$cos\theta = -1 + \frac{2(\gamma_S^d . \gamma_{LV}^d)^{1/2}}{\gamma_{LV}} \ . \quad (3.19)$$

For non-polar liquids, where $\gamma_{LV}^d = \gamma_{LV}$:

$$cos\theta = -1 + 2(^{\gamma_S^d}/_{\gamma_{LV}})^{1/2} \ . \quad (3.20)$$

where γ_S^d and γ_{LV}^d represent the dispersion force contribution of the surface tension for the solid and liquid-vapour interface respectively.

For non-polar liquids on a substrate of known solid surface tension, θ should decrease as the γ_{LV} decrease and become zero below a certain γ_{LV} value. This value is known as Zisman's critical surface tension, γ_c, for the solids [42, 80]. This is demonstrated by the graph of the contact angle of different liquids on the same surface, and it is a smooth plot of $\gamma_{LV}cos\theta$ vs γ_{LV}[82]. An example is the graph of n-alkanes shown in Figure 3.7. Low surface tension solids are described by a critical surface tension, γ_c, which represents an empirical measure of the surface tension of a liquid that spontaneously wets on a given surface [75].This parameter is estimated by measuring the contact angle, θ, of a series of liquids placed on the known solid substrate [80].

A method of measuring the contact angle is using a goniometer, and in [83], they used a goniometer equipped with software designed for calculating the value of contact angles from the shape of an attached air bubble using the Young-Laplace equation. Another method is by using a goniometer with a mounted camera for taking the images of the droplet to measure the contact angle. This type of system is used in this work to measure the contact angle of ink and will be discussed further in Chapter 4. Under ideal conditions and surfaces, the measurement of contact angles is accurate to ±1º and is easy to perform.

The complications associated with the measurement of contact angle are [42]:

- contamination of liquid
- a solid surface that is homogeneous and free of impurities is needed, which is hard to obtain
- contact angles are rarely single-valued quantities, but for a given system, a range of metastable contact angles exist.

The contact angle will depend mainly on a) whether the liquid is advancing over a dry surface or receding from a wet surface, and b) the extent to which the drop is vibrated [82]. Contact angle hysteresis of the advancing and receeding angles, is most noticeable with chemically and/or geometrically heterogeneous surfaces [42]. The impact and spreading of solution drops on a solid substrate is important in many technical applications such as printing, painting, and spraying of pesticides [84].

Homogenous surface angle is independent of the volume of the drop. According to Myers, the relationship between the theoretical (i.e. for completely smooth surfaces) contact angle and the actual contact angle is given by:

$$r = \frac{cos\theta^{exp}}{cos\theta^{smooth}}, \tag{3.21}$$

where r = the roughness factor of the surface and the value of r can be estimated by Atomic Force Microscopy [85]. From the above equation, contact angle measurements are another source of information about surface roughness.

CHAPTER 4: EXPERIMENTAL PROCEDURE

4. EXPERIMENTAL PROCEDURE

4.1. INK PREPARATION

For the experiments performed in the broader project, screen-printing was used as a method of ink deposition on paper substrates. Pastes for screen printing contain an organic binder, silicon nanopowder and an organic solvent [3]. Not only will the method of the preparation for the paste affect the printed structure, and subsequently the electronic properties of the material, but the pastes must have certain rheological properties before printing. A highly viscous paste will dry on the screen and a low viscosity paste will bleed into the paper substrate.

The amount of binder included in the ink composition depends on the final application of the printed layer, but in general, there is a minimum amount required to maintain integrity and to obtain sufficient adhesion to the substrate. At the same time the binder content has to be kept as low as possible to avoid separation of the nanoparticles and restriction of the charge carrier movement [67]. The other function of the liquid components is to control the viscosity of the inks for printing. A solvent is therefore added to the ink to give appropriate pseudoplastic properties to the ink before screen printing [86].

The following materials were used for the preparation of the silicon nanoparticle functional inks. The binder, solvent and silicon nanoparticle powder were used as received, without any chemical modification. The viscosity values of the individual liquid components were determined using a Viscolite viscosimeter.

Binder:

- Flexiclear is a commercial acrylic emulsion binder that is produced by Marchem (Pty) Ltd, Cape Town, South Africa. It is commonly used for screen printing designs on textile products such as T-shirts. It has a measured viscosity value of 0.21 Pa.s, contains approximately 60 % water, and has a white gel-like appearance.

Solvent:

- 1,2 propandiol, referred to as glycol in this work, is a diol alcohol prepared by the hydration of propylene oxide, resulting in a mixture of 1,2 propanediol and dipropylene glycol [87]. It has a measured viscosity value of 0.056 Pa.s and is miscible in water, acetone and chloroform. This solvent is hygroscopic, i.e. it takes up and retains moisture at certain temperature and humidity conditions.

Powder (functional material):

- Silicon nanopowder was bought from MTI Ltd, Richmond, CA. The powder has a particle size of 50 nm and a narrow particle size distribution [88].

The binder, powder and solvent were used in different combinations to prepare the silicon nanoparticle inks. The inks were all hand-mixed by sequentially adding powder to the binder and thinning with the solvent when necessary.

The following compositions of inks were prepared in order to observe the effect that varying the amount of solvent and particle loading has on the rheological properties, surface properties, printability, and electrical performance of the inks. The experiments are separated into two sections: solvent and powder variation inks, as indicated in tables 4.1 and 4.2 respectively.

Table 4.1. The table of solvent variation of the silicon nanoparticle inks with the same amount of binder and powder.

Mass of flexiclear binder (g)	Mass of Si powder (g)	Volume of glycol (µL)
0.25	1.0	1500
0.25	1.0	1750
0.25	1.0	2000
0.25	1.0	2250
0.25	1.0	2500

Table 4.2. The table of the variation of powder added into silicon nanoparticle inks with the same amount of binder and solvent.

Mass of flexiclear binder (g)	Mass of Si powder (g)	Volume of solvent (µL)
0.25	0.5	2000
0.25	0.75	2000
0.25	1.0	2000
0.25	1.25	2000
0.25	1.5	2000

After preparation, the inks were characterized for rheological behaviour and contact angle, as discussed in section 4.2, and the results are represented in Chapter 5.

4.2. INK ANALYSIS AND CHARACTERIZATION

The flow and adhesion properties of the inks are important in screen-printing as the packing of particles is dependent on the rheological properties of the inks. Different inks behave differently on the screen because of the differences in viscosity and surface tension, therefore the rheological properties of the paste are important in obtaining good screen printing quality [4]. Rheology can be used as a measure of the printability of the material as the sample can be put through the same shear loading conditions, as it would be during screen printing.

For this reason, the rheological measurements were performed on the silicon nanoparticles inks used for printing electronic devices. The inks are non-Newtonian and the focus of the experiments performed was on the behaviour of the inks at different shear rates. Rheological characterization of the inks was performed at the National Centre of Nano-Structured Materials (CSIR, Pretoria).

4.2.1. Rheometry

Figure 4.1, is a photograph illustrating the important features of the measuring system of a rheometer [48]. Such instruments are used for the rheometry of non-Newtonian fluids. The behaviour of non-Newtonian fluids cannot be defined by a single viscosity value; therefore, rheological measurements were performed under varying forces and strain loading.

The rheometer that was used for analyzing the flow behavior of the silicon nanoparticle inks is the *Anton Paar Physica MCR 501 rheometer* equipped with an electronically commutated motor drive with an air bearing.

The rheometer parameters for the characterization of the samples were:

- Temperature = 25 ℃
- Measuring system = 25 mm parallel plates and 50 mm cone-plate

- Trim position = 0.6 mm
- Measuring position = 0.5 mm
- For the cone-plate system, the measuring position is 0.3 mm and the cone angle of 0.4 °

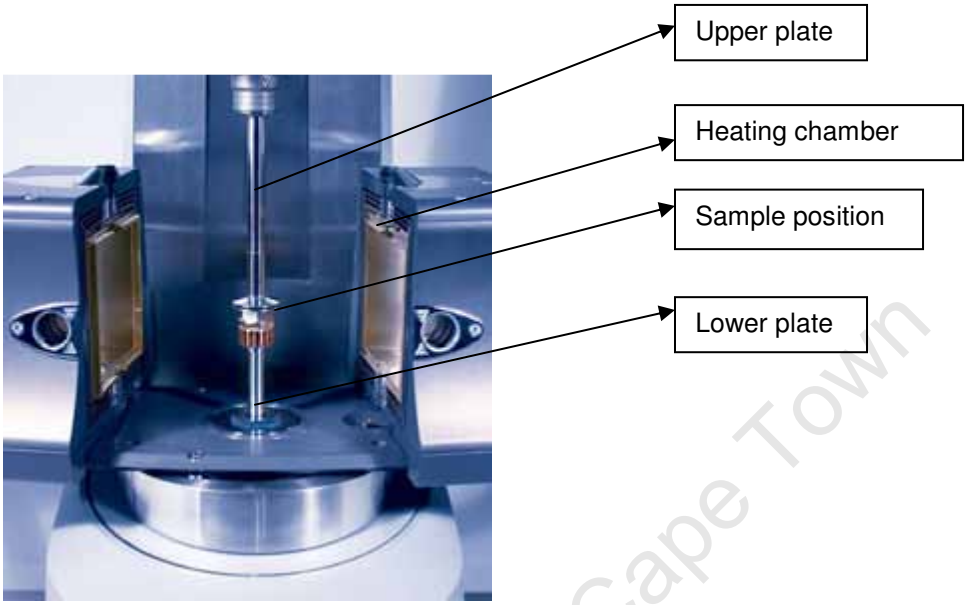

Figure 4.1. The inside of the rheometer with the heating chamber and 25mm parallel (lower and upper) plates [48].

For the measurement, the sample is placed on the lower plate, the upper plate is lowered to a pre-determined measuring position and any excess material is trimmed before the measurements starts. The plates were cleaned with acetone before and after each measurement.

Table 4.4 is taken from the Rheology Handbook by Mezger, [22], and it demonstrates the types of tests that can be performed using a rheometer on different types of materials.

Table 4.4. The rheological measurements for different types of materials [22]

Liquid		**Solid**	
(ideal-) viscous Flow behaviour Newton's law	**Viscoelastic Flow behaviour** Maxwell's law	**Viscoelastic Deformation behaviour** Kelvin / Voigt's law	(ideal-) elastic Deformation behaviour Hooke's law
Flow /viscosity curve	Creep tests, relaxation tests, **oscillatory tests**		

The areas that are written in bold represent the liquids and solids that do not behave in an ideal Newtonian manner, and these tests were performed on the silicon nanoparticle inks. The following three rheology tests were performed for each silicon nanoparticle ink.

4.2.2. Amplitude sweep

Amplitude sweep tests, i.e. an oscillatory test with variable amplitude and constant frequency values, were performed in order to determine the linear viscoelastic (LVE) range of a material. The LVE range of materials is the strain range below which the material deforms linearly and the storage and loss moduli vs. strain rate curves show a constant plateau. The measurements were performed under controlled shear strain (deformation) with the strain amplitude as the variable and a constant angular frequency of 1 Hz. The determination of the LVE range is important as the rheology results are only valid when the material is within the linear viscoelastic region [4]. This LVE range value is a basis for the frequency sweep test and any other tests that are to be performed as they all have to be carried out within the LVE range [22].

The LVE range is calculated from the raw data using a software application, by calculating the point at which the material starts to deform no-linearly. The strain value for the LVE that is obtained from the amplitude sweep measurement is used as a parameter for the frequency sweep and thixotropy tests, so the test must be carried out for each individual sample.

4.2.3. Frequency sweep

A frequency sweep is an oscillation test with a variable frequency and constant amplitude, using the LVE range value obtained from the amplitude sweep. The test evaluates the time-dependent behaviour of the sample. At low frequency it simulates long term behaviour, whereas short-term behaviour is simulated by the higher frequencies [22]. The outcomes of this test are the storage and loss moduli of the sample and their dependence on angular frequency. The loss and storage modulus will give an idea about the extent of the viscoelasticity of the material, the time-dependent deformation, and the stability of the dispersion. Depending on the value of the storage modulus in relation to the loss modulus it can be deduced whether the dispersion is stable against separation [42].

4.2.4. Thixotropy test

A 3-Interval Thixotropy Test (3ITT) was used to simulate the shear rate that the ink goes through during the screen printing process. The ink is put through three intervals at different shear rates and times in the sequence: *oscillation – rotation – oscillation*. At high shear rate, the rotation causes more effective structural deformation than oscillation, which is the reason why the second interval is rotation. Most screen printing machines reach a shear rate of up to about 1000 s^{-1} when the squeegee pushes the paste to penetrate through the mesh. Therefore attention need to be paid to the behaviour of the pastes at high shear rates [4].

The parameters used for the 3ITT were:

1st interval: Oscillation in the LVE range for 100 seconds with 5 measuring points.

2nd interval: Rotation at high shear rate, γ = 813 s^{-1}, for 5 seconds with 10 measuring points.

3rd interval: Oscillation in the LVE range for 1100 seconds with 100 measuring points.

The shear rate for the 2nd interval was calculated using the equation of Tanaka et al [89], which was originally used to determine the shear rate of the screen-printed catalytic electrodes for MEMS-based fuel cells. This equation is based on the parameters of the screen printing process,

$$\gamma = {}^{2vt}/_{\omega^2} \qquad (4.1)$$

where γ is the shear rate,

v is the squeegee speed,

t is the thickness of the screen, and

ω is the opening size on the screen.

In our system, the above parameters were measured as v = 200 mm/s; t= 62 µm and ω= 30.5 µm, and therefore the calculated shear rate of the squeegee during printing is γ = 813 s^{-1}.

4.2.5. Contact angle measurements

The contact angle of a liquid, which is the angle that a droplet of the liquid makes with a surface (Figure 4.2), is a quantitative measure of the wetting of the solid substrate by the liquid [75]. The contact angle of a liquid can be used to determine the fluid's surface tension with a given substrate by using Young's equation. In this project, the contact angle of the inks is used as a means of predicting the printability of the ink.

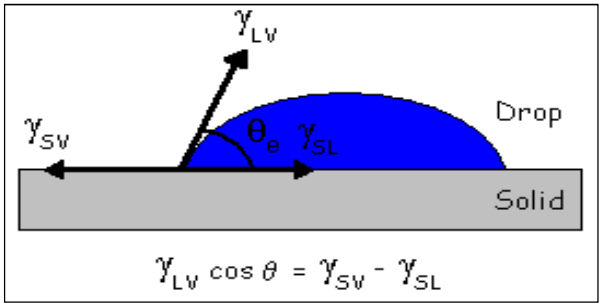

Figure 4.2. An illustration of the forces acting on a droplet of liquid on a solid substrate.

Young's equation represents the mechanical equilibrium condition of a droplet under the action of the three interfacial tensions [8, 42, 75, 82] :

$$\gamma_{SV} = \gamma_{SL} + \gamma_{LV} cos\theta \ , \qquad (4.2)$$

Contact angle measurement using a goniometer is a non-destructive technique which uses very little material. The contact angles of silicon nanoparticle inks were measured using a home-built goniometer. The system consists of a webcam mounted on a stand and sample stand in front of the camera for placing samples, see Figure 4.3.

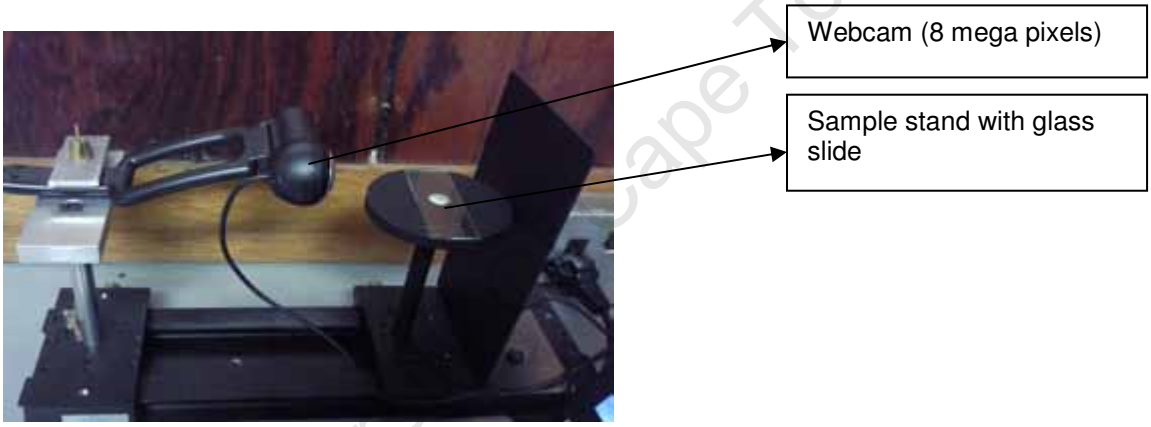

Figure 4.3. The home-built goniometer for contact angle measurements of silicon nanoparticle inks and binders.

The measurement process is as follows:

- A small droplet of the ink from the bulk solution was placed onto a cleaned (with acetone and ethanol) glass slide.
- The slide is then mounted onto the sample stand, with care to avoid vibrating the droplet.
- Quickcam software was used in focusing the image to get the best picture for measuring the angle.
- The image of the sample was taken with the webcam. On average 5 pictures were taken for the same sample at different zoom and focus settings.

- Image J software was used in measuring the contact angle, this is measured by drawing a line parallel to the liquid/solid interface and joining this with a line tangent to the surface of the droplet as shown in Figure 4.4 for the contact angles below and above 90°.

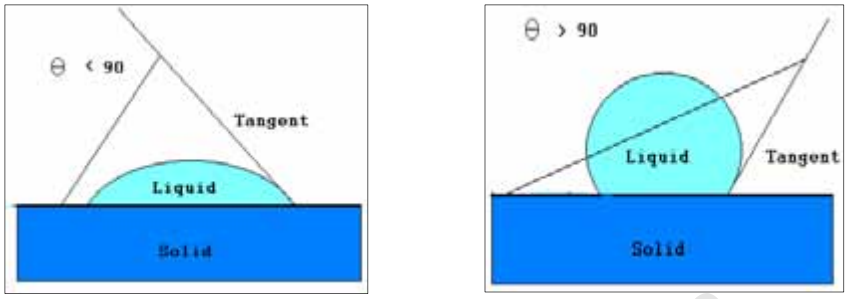

(a) (b)

Figure 4.4. Determination of contact angles between a liquid and a solid substrate (a) contact angle less than 90°, (b) contact angle greater than 90°.

4.3. SCREEN PRINTING OF SILICON NANOPARTICLE LAYERS

The inks were prepared again in the same manner, for screen printing. Screen-printing, which has been extensively discussed in Chapter 2, has been used in the production of thick-film electronics materials, e.g. superconductors, solar cells, ceramic films, etc [90]. Below is a detailed discussion of the screen printing equipment at University of Cape Town, as well as its operational parameters.

The screen printing machine used is an *ATMA AT* series semi-automatic printer, which has the following components, shown by the photograph in Figure 4.5:

- flat bed with vacuum for placing the substrates
- screen frame upon which the screens are mounted
- squeegee and flood bar for covering the screen and pushing the ink through the mesh
- The machine has a touch screen for ease of operation.

The machine was operated with a print speed of 200 mm/s and off-contact distance of 0.1 mm. The screen mesh tension, squeegee pressure, the off-contact distance and the screen peel after printing, can all be adjusted to produce a layer with the desired thickness and registration.

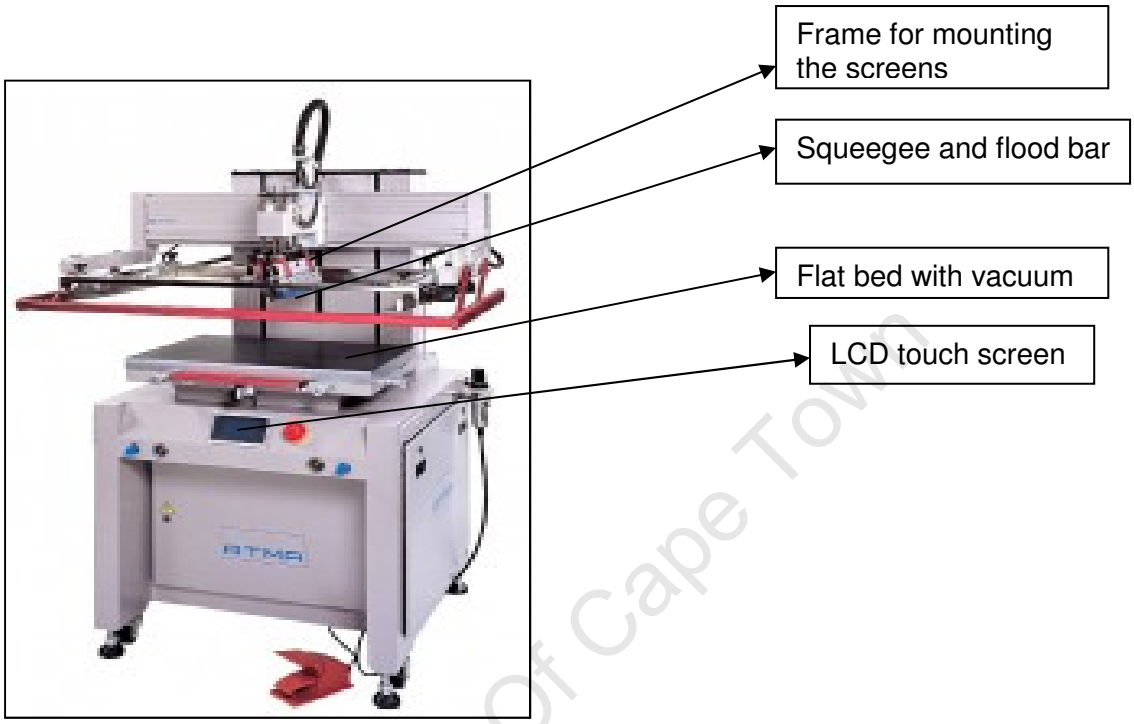

Figure 4.5. The ATMA screen printing machine used for printing functional inks.

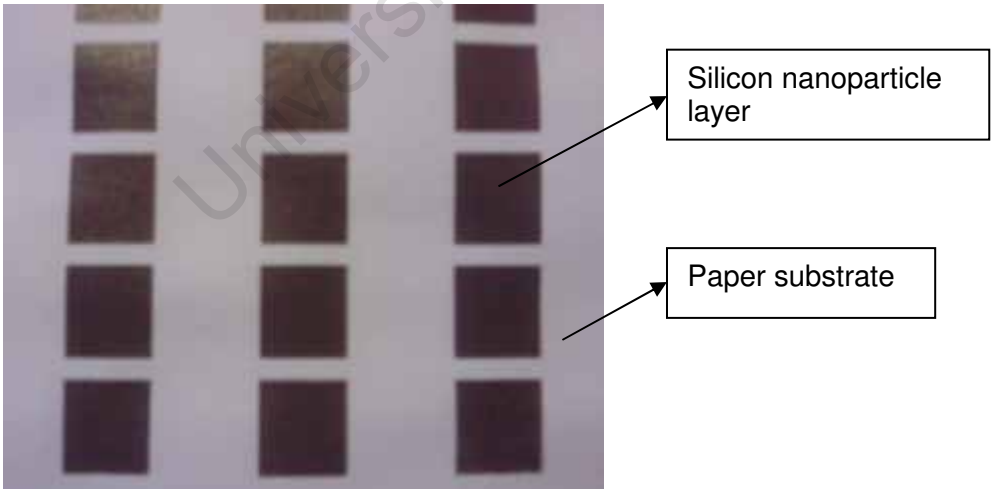

Figure 4.6. The layers of silicon nanoparticle ink that were screen printed using the above procedure. The squares are 9 cm x 9 cm in size and on average 32 squares make up the design.

4.4. PRINTED LAYER CHARACTERIZATION

The silicon nanoparticle inks were screen printed immediately after preparation and left to air-dry for 24 hours before further characterization. The cured printed layers were characterized using optical microspopy and scanning electron microscopy (SEM) to observe their morphology and print quality. The samples were also characterized for electrical performance to determine the resistance and photo response of the silicon nanoparticle layers.

4.4.1. Surface morphology

The optical microscope that was used was the Photomakroskop M400V instrument equipped with a digital camera that uses the Axio Vision 4.4 camera software. The cured printed layers were analyzed without modification, see Figure 4.6, and they were viewed at X16 magnification.

For better resolution, scanning electron microscopy was used to analyze the samples. This technique gives information about the surface characteristics, morphology and topography of the sample at a much higher magnification that the optical microscope. The advantages of using scanning electron microscopy over optical microscopy are the greater depth of focus, the direct observation of the external form of real objects, the ability to switch over a wide range of magnification, and the large space available for dynamic experiments on the specimen [91].

The SEM equipment used was a Leica Stereoscan S440i, at the Electron Microscopy Unit, University of Cape Town, with tungsten filament as the electron source, beam settings was 20keV acceleration potential and a beam current of 800pA. Imaging was primarily achieved by using a secondary electron detector. The samples for SEM were prepared by cutting the printed silicon nanoparticle layers, shown in Figure 4.6, into small samples of 5mm x 8 mm blocks with a surgical blade.

Two samples for each ink were prepared to view the cross-section and the surface of the printed layers. The two specimen were mounted on standard SEM stubs using carbon glue, with one sample placed flat on the stub for surface view and the other sample glued vertically for cross-sectional view. The sample were then coated with approximately 5nm of gold to ensure conductivity.

4.4.2. Electrical Characterization

The printed silicon nanoparticle layers were characterized for photo response and resistance using a Keithley 4200 semiconductor characterization system (SCS). The SCS is equipped with a double Faraday cage to eliminate interference [92], a sample stage inside the cage and probes made of either gold or tungsten. The photo response of the printed layers was measured by switching a fluorescent light of intensity 21.3 Wm^{-2}, on and off in 300 s and 600 s intervals to a total measurement time of 1 800 s [92]. The current and voltage measurements were performed separately and were measured during the “light on” and “light off” intervals.

The sample for the photoresponse characterization was a silicon layer printed between two commercial conducting inks, DuPont 5000 silver at the bottom, and DuPont 7102 transparent conducting oxide on top.

The resistance of the printed layers was measured using the Keithley 4200 SCS in current and voltage sweep mode. Figure 4.7 is a photograph of a typical printed resistance sample prepared by printing silicon nanoparticle ink on top of the printed silver contacts. The resistors were connected with the probes in the same manner as the photo response measurements and the system was set for voltage sweep from -50 V to 50 V for two point-resistor measurements with a sweep delay and hold time of 0.01 s.

In total 86 resistors were measured, with all the ink except the ink containing 1.5 g of powder producing 10 resistor samples each.

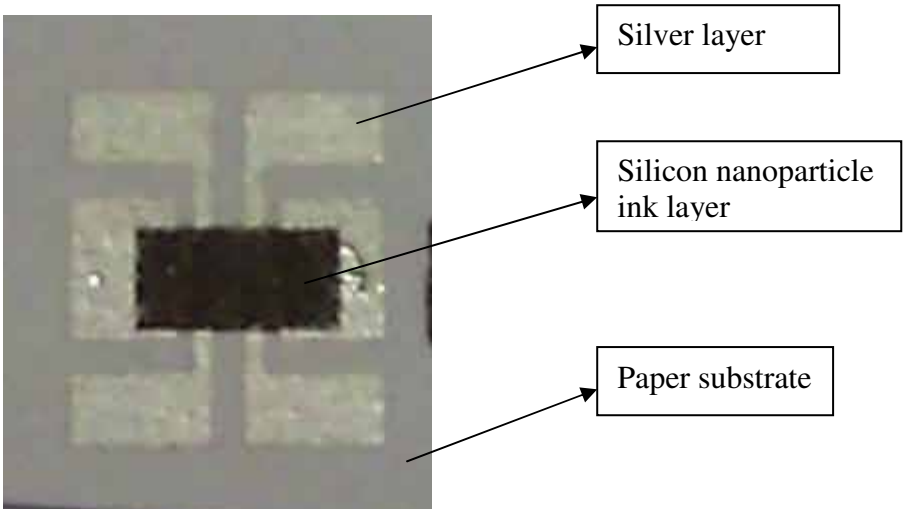

Figure 4.7. The printed resistor device with the silicon nanoparticle layer strip of 1.1 x 0.7 cm dimensions.

CHAPTER 5: RESULTS

5. RESULTS

5.1. RHEOLOGY

After preparation, the inks were characterized for rheological, surface and electrical properties. The method that was used in selecting the different particle loading and solvent additions was based on one ink that contained 0.25g binder; 1.0g powder and 2000 µL solvent. This ink showed good electrical properties and printed very well but it was prepared with no knowledge of the rheological properties and was judged for printability based on the consistency and contact angle it made with a glass slide. It was then seen as important to understand the rheological properties of this ink by conducting measurements on the inks containing varying amounts of solvent and particle loading based on the above-mentioned ink. This experiment resulted in the preparation of 9 inks. The rheological behaviour is explained in detail below, with more focus on the determinination of the linear viscoelastic (LVE) range and time-dependent behaviour.

5.1.1. Solvent variation

In this process the amount of powder and binder in the inks were held constant, but the amount of solvent was varied from 1500 µL to 2500µL, in 500 µL increments resulting in the preparation of the 5 inks, listed in table 4.1.

As explained in section 4.2.1, amplitude sweep tests are performed to determine the strain below which the material does not deform because all the other rheology measurements are performed below this range. The data obtained from amplitude sweep is the storage (G') and loss (G'') moduli as a function of strain (shear rate). The results are plotted in Figure 5.1.

The curves in Figure 5.1 show the same behaviour in that there is a slight increase of both G' and G''at low strain, then both decrease at higher strain values. The decrease at high strain values is stronger for G' than for G'', and this behaviour is most pronouced for the ink containing 1750 µL of solvent.

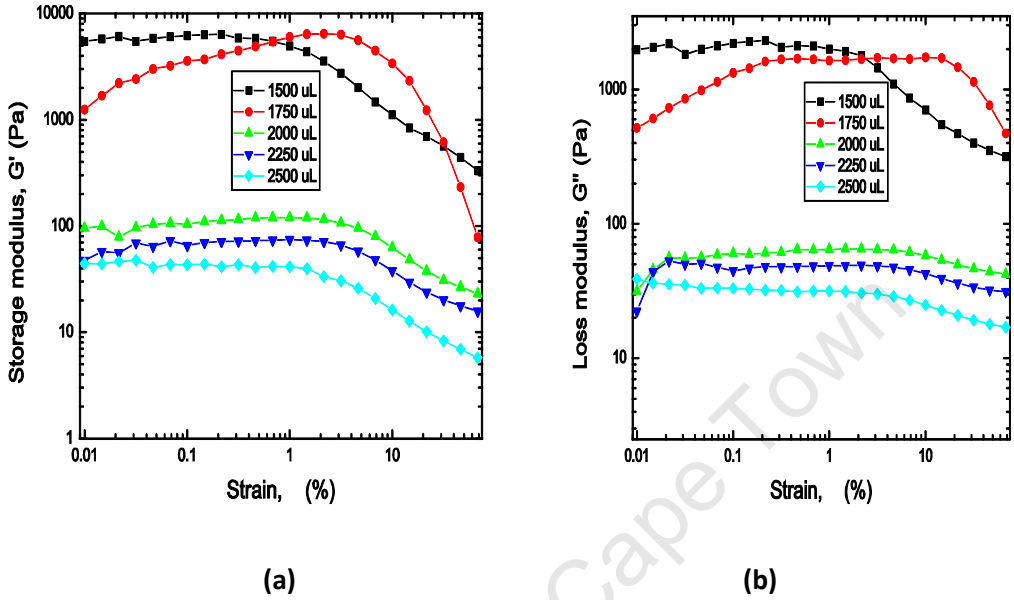

(a) (b)

Figure 5.1 (a) The storage modulus (G') and (b) loss modulus (G'') of the silicon nanoparticle inks containing different amounts of solvent form amplitude aweep measurements

The inks all exhibit shear thinning behaviour, indicated by decrease in G' and G'' with increasing strain, with this behaviour being more prominent for the inks contaning low solvent amounts. The behaviour of G' and G'' for the sample containing 1750 µL of solvent is different from all the other inks, in that the curves show a clear increase until 2 % strain and then decrease sharply, resulting in the G' and G'' curves forming cross-over points with the curves for the ink containing 1500 µL of solvent. There is a large difference in the magnitude of the moduli between inks containing low amounts of solvent and high amounts of solvent which result in the curves grouping into two regions in the figures.

There is a systematic decrease in the ratio of G' to G''. For the inks containing low amounts of solvent the ratio is 3, whereas for inks containing high amounts of solvent, the two moduli are approximately equal. The relationship between G' and G'' is such that for low strain values, the storage modulus dominates over the loss. Where the moduli start to decrease there is a cross-over point, beyond which the G'' dominates over the G' at high strain values. Below this cross-over point, the inks show elastic characteristics and afterwards the inks are more viscous [22]. Table 5.1 shows the values for these cross-over points for all the inks. It is observed that as the amount of solvent in the ink is increased, the cross-over point occurs at lower strains.

Table 5.1. The cross-over point strain values of G' and G''.

Volume of solvent (µL)	Cross-over point (% strain)
1500	100
1750	18
2000	12
2250	7
2500	3.5

Flow curves represent the shear stress vs. strain (shear rate) relationship of materials, as shown in Figure 5.2 for the silicon nanoparticle inks containing different amounts of solvent. The shear stress and strain relationship for all the inks is indicative of shear thinning behaviour, shown by the decreasing in slope of the curve with an increasing strain. This behaviour was observed more strongly in the inks containing low amounts of solvent.

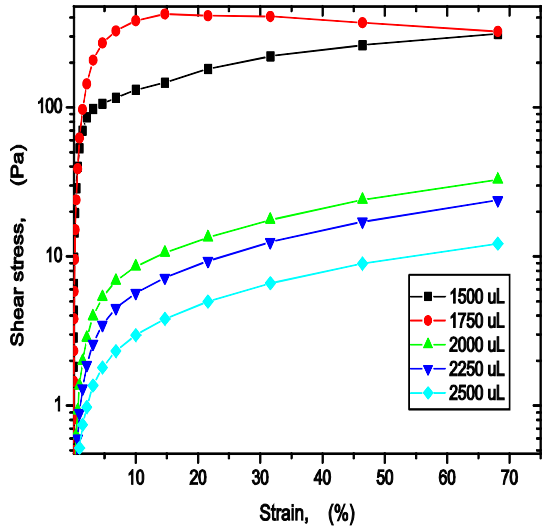

Figure 5.2. The flow curve, shear stress (τ) vs strain curves (γ) of I-Si inks with varying amounts of solvent.

As with the amplitude sweep measurements in Figure 5.1, the curves in Figure 5.2 show a large difference in the shear stress between the inks containing 1750 µL and 2000 µL of solvent. The samples containing 1500 µL and 1750 µL of solvent show a rapid increase in shear rate at low strain in comparison to the inks containing 2000 µL to 2500 µL of solvent, where the increase is more gradual. The curve for the ink containing 1750 µL of solvent has a negative slope for strains higher than 15% where there is a maximum. This behaviour is observed in materials with creep, i.e. a negative slope for the stress vs. strain curves at high strain values. The general behaviour of these flow curves is similar to the Windhab model flow behaviour [22]. The fitting of the data to this model will be discussed in more detail in Chapter 6.

Figure 5.3 represents the behaviour of the complex viscosity of the inks with a change in angular frequency. The raw data for plotting the curves was obtained from the frequency sweep measurements. The curves show a decrease in complex viscosity as the angular frequency increases, which is normally observed for shear thinning materials [22, 71]. From the curves in Figure 5.3, the lower the amount of solvent added to the inks the more shear thinning the behaviour exhibited by the inks.

The complex viscosity values for the inks congregate towards a similar value for angular frequencies of more than 100 Hz.

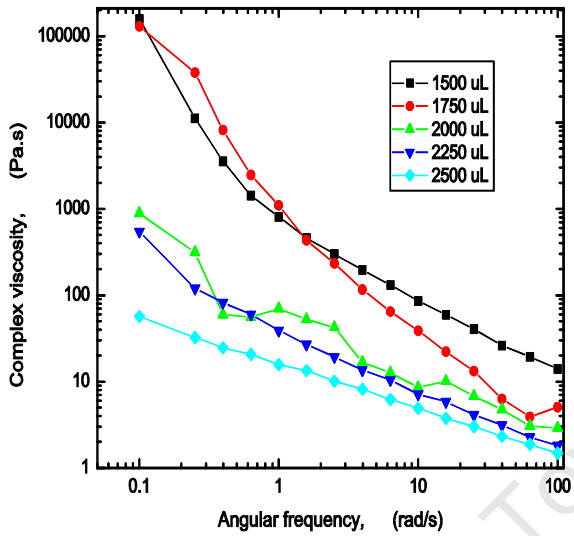

Figure 5.3. Complex viscosity of the inks containing different amounts of solvent with the change in frequency.

The decrease in complex viscosity with the angular frequency is linear in a logarithmic representation for the sample containing 2500 µL of solvent, suggesting a power law behaviour or Ostwald / de Waele model as often applied for the rheology of colloids [22, 71].

Frequency sweep measurements were performed for each ink using the LVE range strain values obtained from the individual inks and the curves are plotted in Figure 5.4. These curves represent the frequency dependence of the storage and loss moduli. As with the amplitude sweep data, there is a large difference in G' and G'' for the ink containing 1750 µL and 2000 µL of solvent at low strain values. The general trend is that the higher the amount of solvent added into the ink, the lower the values of G' and G''.

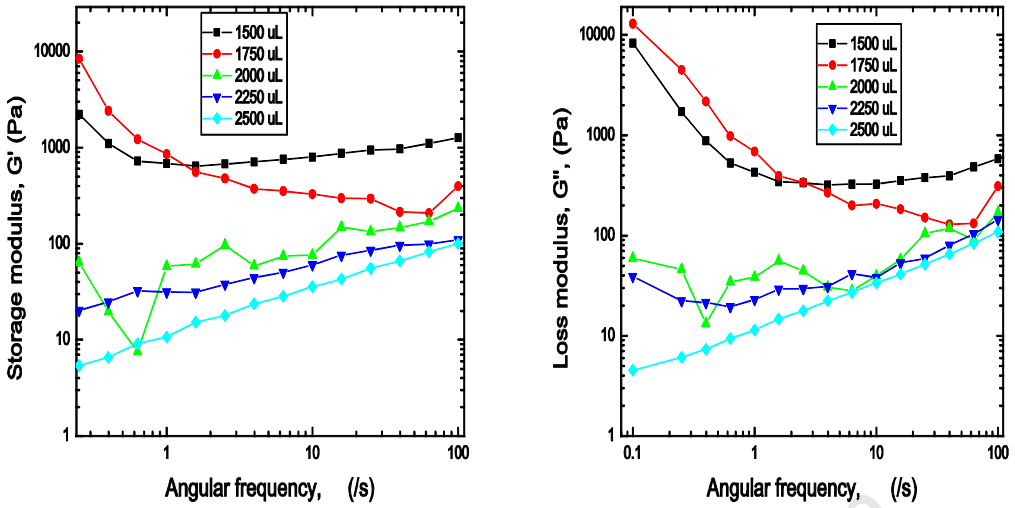

Figure 5.4 .(a) The change in storage modulus and (b) loss modulus with frequency for the inks containing different amounts of solvent, from frequency sweep.

For the inks containing low amounts of solvent, i.e. 1500 µL and 1750 µL, both the G' and G'' decrease at low angular frequencies and start to increase around 1 Hz and 80 Hz respectively. This is in contrast with the moduli for the inks containing 2000 µL of solvent and more, which increase throughout the entire frequency range. The storage modulus is higher than the loss modulus for all the inks except the ink containing 2500 µL of solvent. The two moduli for the ink containing 2500 µL are plotted together in Figure 5.5.

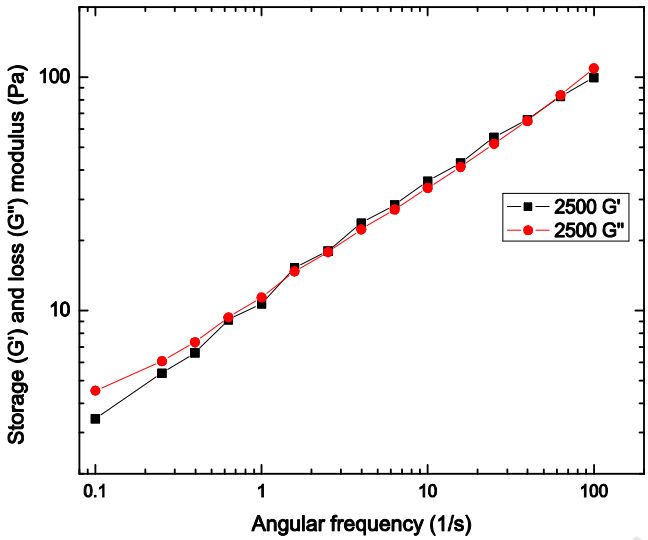

Figure 5.5. Storage (G') and loss (G'') moduli from frequency sweep data. The curves are for one sample with 2500 µL solvent added.

The storage and loss moduli curves of the ink containing 2500 µL of solvent are close for angular frequency more than 1 (/s), which indicates a stable dispersion [22].

The values of G' for all the inks are plotted against G'' values in Figure 5.6, as a function of frequency in an analogous manner to the Cole-Cole plot [93, 94].

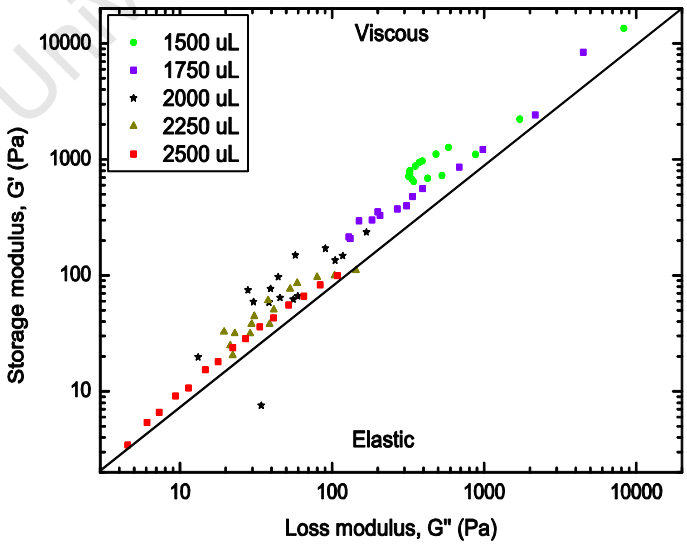

Figure 5.6. G'' vs G' relationships for all the inks with varied amounts of solvent.

The area above the middle line represents the viscous characteristics of the ink, and the lower part represents the elastic behaviour [94]. There is no transition from the lower to the upper region for all the inks and they all remain in the upper or viscous region throughout the entire frequency range.

Thixotropy measurements were performed in order to simulate the mechanical load that the silicon nanoparticle inks undergo during printing. These were carried out according to the procedure in section 4.3 where the shear rate is varied from low to high and the complex viscosity, storage and loss moduli are measured as a function of time. The curves in Figure 5.7 represent the complex viscosity, η^*, with time. The two vertical lines in Figure 5.7 around 100 s indicate the deformation stage of the measurement when the shear rate was increased to 813 /s for 5 seconds. Before and after this deformation stage the shear rate was low, as described in section 4.3.

Figure 5.7 represents the complex viscosity of the inks at different amounts of solvent. The inks containing 1750 µL of solvent and above show a decrease in viscosity at low shear rates before deformation, but the ink containing only 1500 µL exhibits an increase in viscosity before deformation. After deformation all the inks show shear thickening behaviour (rheopexy) for low shear rate. However, the time it takes the inks to recover increases as the amount of solvent is increased, from almost instantaneously for the ink with 1500 µL of solvent, to 500 s at the highest dilution. The ratio of the initial, $\eta^*_{(0)}$, and final, $\eta^*_{(1100s)}$, complex viscosities decreases as the amount of solvent is increased indicating that the inks are more shear thickening after deformation.

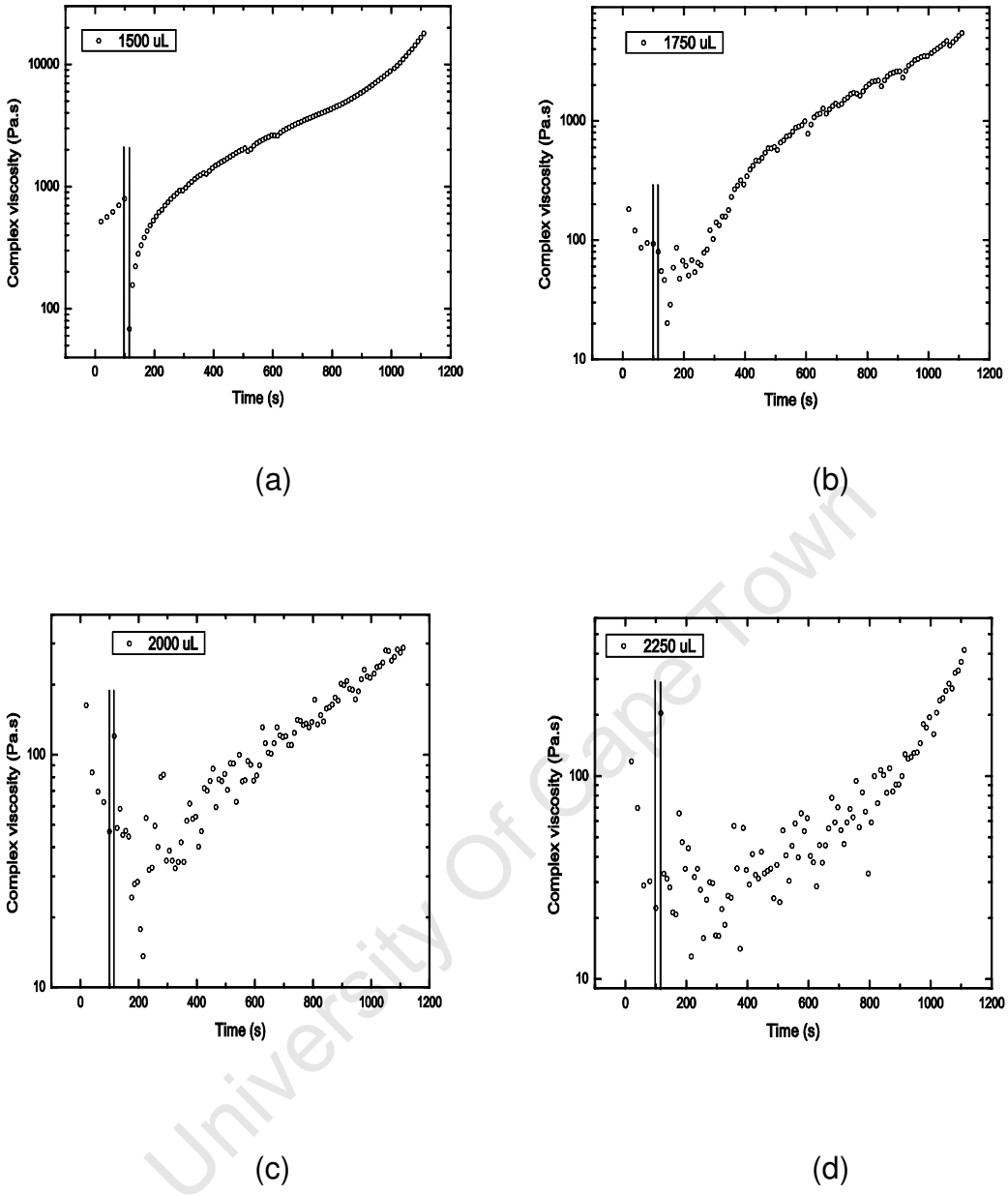

Figure 5.7 The complex viscosity curves from thixotropy measurements of the inks containing different amounts of solvent from (a) 1500 µL, (b) 1750 µL, (c) 2000µL and (d) 2250µL.

Contact angle measurements

The contact angles of the silicon nanoparticle inks were measured as described in section 4.1.2, for each ink immediately after preparation. The ink was forced onto the slide, which gave a measurable contact angle with the surface. The images of the droplets for the contact angles of the inks are presented in Figure 5.8 and the measured contact angle values are plotted as a function of the amount of solvent in Figure 5.9.

The images in Figure 5.8 show the change in the shape and size of the droplets with the change in the amount of solvent added into the ink. The droplet for the ink with the lowest amount of solvent, i.e. image (a), is elongated and irregular in comparison to the droplets of the other inks which form regular, round shapes as the amount of solvent in increased. In terms of their size, the droplet of the ink containing 1750 µL of solvent, image (b), is small in comparison to the other droplets.

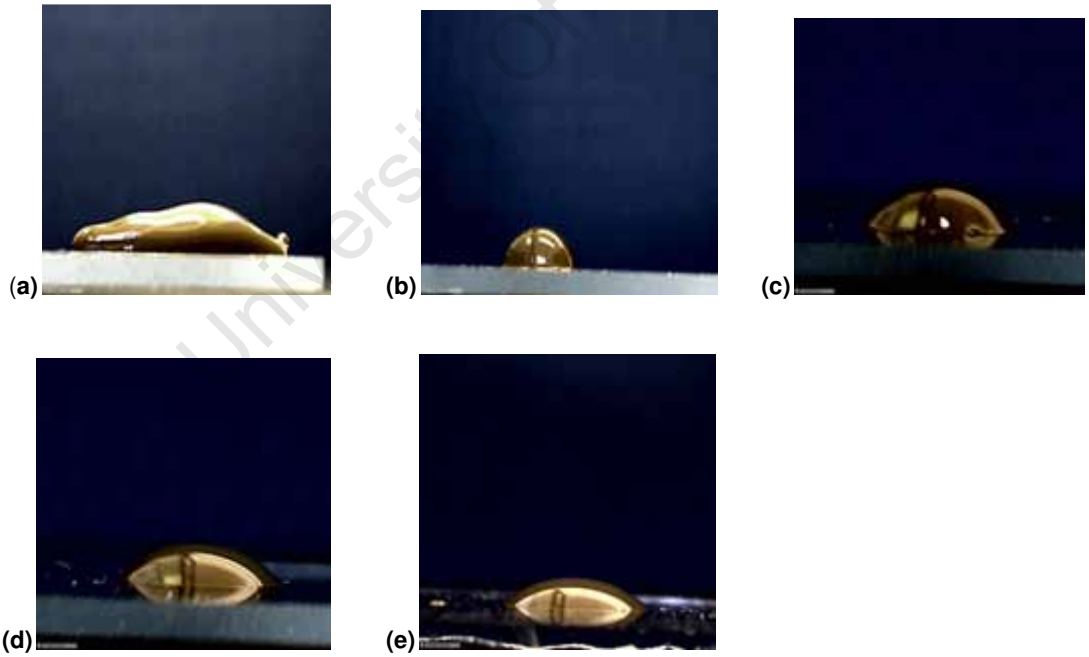

Figure 5.8. The images above are of the inks droplets with different amounts of solvent, (a) is 1500 µl, (b) 1750 µl, (c) 2000 µl, (d) 2250 µl and (e) is 2500 µl of glycol.

The change in contact angle with an increase in the amount of solvent in the inks is confirmed by the measured values in Figure 5.9. The errors on the individual measurements are small compared to the size of the symbols.
The contact angle values decrease as the amount of solvent in the inks is increased.

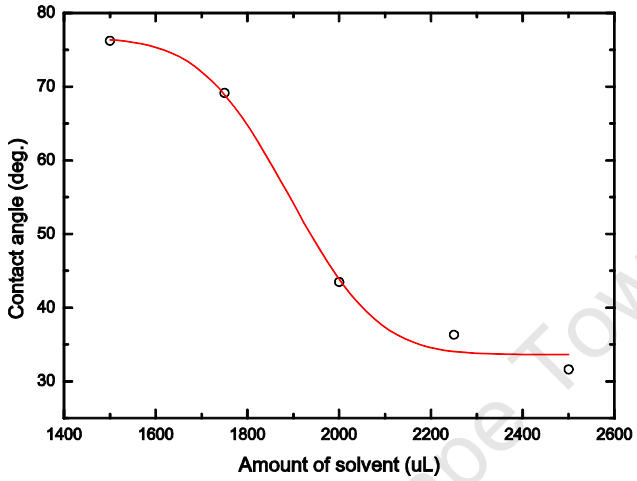

Figure 5.9. Contact angle of the inks with a glass slide as substrate, the inks had varying amounts of solvent.

The dependence of the contact angle on solvent amount forms an S-shaped curve with the steepest change between the sample containing 1750 µL and 2000 µL, and saturation at the high solvent loading.

5.1.2. Powder variation

Inks were prepared from the same amount of binder and solvent, but in this case the particle loading was varied as described in section 4.1.2. The amount of powder ranged from 0.5 g – 1.5 g of powder in 0.25 g increments. Amplitude sweep tests were performed for all the ink to determine the linear viscoelastic range of the samples.

The curves in Figure 5.10 show the storage modulus (G') and loss modulus (G'') of silicon nanoparticle inks as a function of strain at different particle loadings. For low particle loading inks there is a slight increase in both moduli at low strain up to 5% strain, and then decrease. The moduli for the ink with the highest particle loading, 1.5g, exhibit a strong increase, peaking around 5 % strain and then decrease drastically.

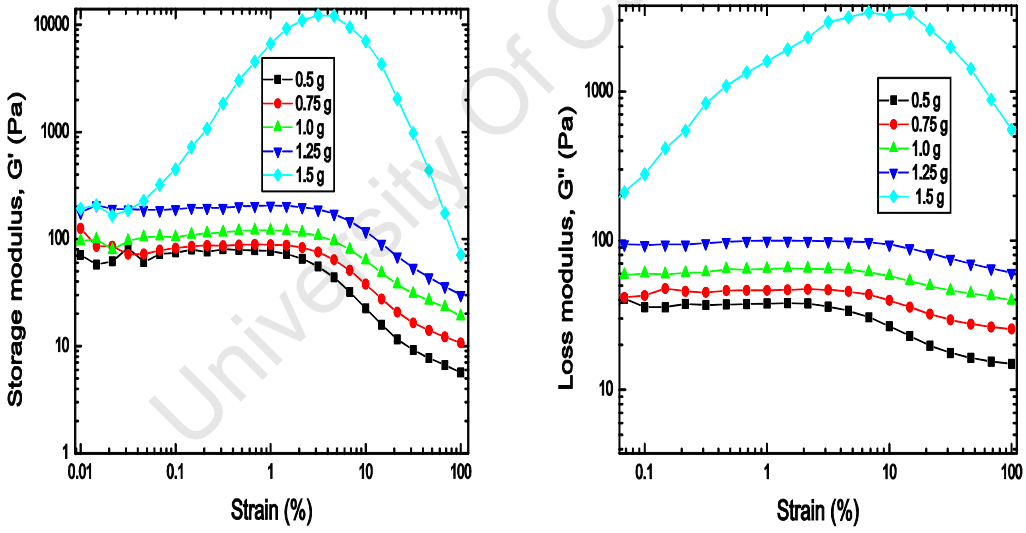

(a) (b)

Figure 5.10. (a) The storage modulus (G') and (b) the loss modulus (G'') of inks with different particle loading, from amplitude sweep data.

All the inks show shear thinning behaviour at high strain, i.e, the G' and G'' values decrease with an increase in strain [22]. Generally, throughout the whole strain range, both moduli increase with particle loading. However, at low strain, the storage moduli of the inks containing 1.0 g of powder or less cluster around the same value of 100 Pa. In contrast, the loss moduli increase systematically with particle loading.

The ratio of G' to G'' for all the inks is approximately 2:1 at low strain values, where G' dominates over G'' (i.e. G' > G''). As for the inks containing different amounts of solvent, it is observed that the rate of decrease of G' with strain is higher than that of G'' which results in a cross-over point so that at high strain G'' dominates over G'. This point depends on the particle loading and is given in table 5.2 for the different inks.

Table 5.2. The cross-over point strain values of G' and G''.

Particle loading (g)	Cross-over point (% strain)
0.5	6.5
0.75	8.5
1.0	10
1.25	15
1.50	20

This cross-over point occurs at higher strain values for inks with higher particle loading than for those with lower particle loading. In a naive interpretaion this suggests that the inks are more viscous than elastic at high strain, and at low strain they are more elastic than viscous [22]. However the waveform of the response may become non-sinusoidal, and so the exact behaviour depends on exactly where the sample is in the applied strain. The actual moduli should be treated cautiously, particularly around the values of maximum strain when the waveforms are likely to be non-sinusoidal.

The flow curves shown in Figure 5.11 represent the relationship between the shear stress and strain of the silicon nanoparticle inks with different amounts of powder added. Firstly, there is a considerable difference between the shear stress required for the inks with 1.25g and 1.5g powder added, for the addition of only 0.25 g powder, suggesting a critical particle loading in this range [63]. The shear stress for the ink containing 1.5g of powder increases sharply at low strain and peaks at 15% strain before decreasing. This behaviour is not observed at lower particle loading, where the stress exhibits a near exponential increase at high strain.

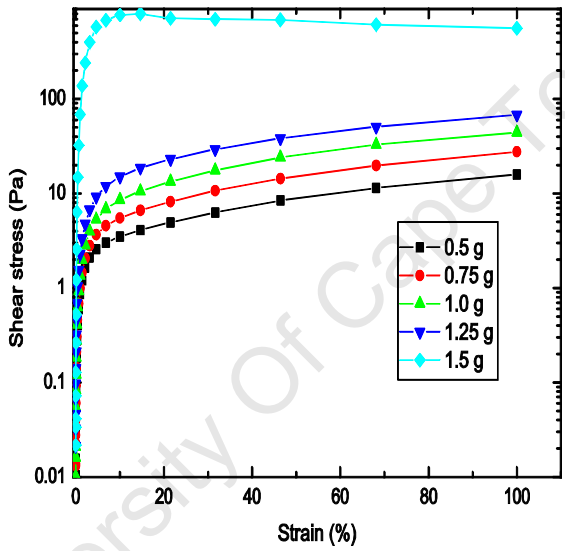

Figure 5.11. The flow curve, shear stress (τ) vs strain curves (γ) of I-Si inks with varying amounts of powder.

In Figure 5.11, with regard to the particle loading, the higher the particle loading, the higher the required shear stress throughout the whole strain range, as expected from the moduli shown in Figure 5.10. Lu, et al. [63] observed a similar behaviour for the effect solid loading on the response to shear stress for aluminium oxide nanoparticle dispersed in poly(methacrylic acid) and poly(acrylic acid). The shape of the flow curve indicates a relationship seen in Windhab model materials [22]. The analysis of the data in terms of rheological models will be discussed in detail in the next chapter.

Frequency sweep measurements were performed to determine the change in complex viscosity, and the storage and loss moduli of the silicon nanoparticle inks with angular frequency. Figure 5.12 shows the behaviour of the complex viscosity of the inks, where the data used to determine the complex viscosity was obtained from frequency sweep measurements. The complex viscosities for all the inks decrease with an increase in angular frequency, indicative of shear thinning behaviour [22, 71]. As expected from the strain dependence of the storage and loss moduli, there is generally an increase in complex viscosity with particle loading.

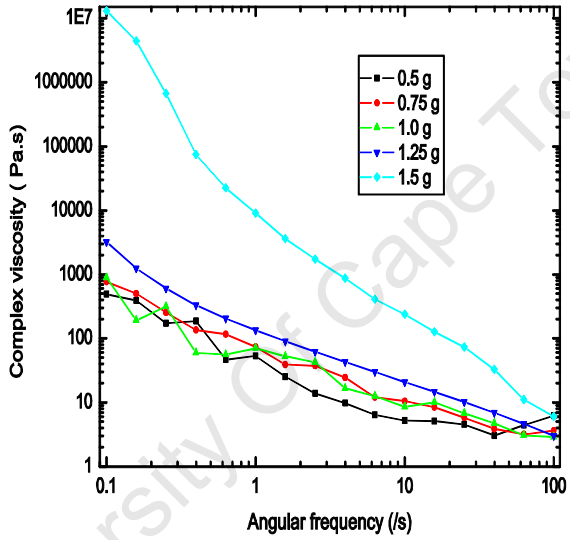

Figure 5.12. Complex viscosity change with angular frequency for different particle loading.

At the highest particle loading, the inks are more shear thinning, i.e. there is a substantial decrease in viscosity with increasing angular frequency, than at lower particle loading. In the high frequency limit, greater than 100 Hz, the inks have similar viscosities around 5 - 10 Pa.s. The logarithmic plots for the inks containing less than 1.25 g of powder are approximately linear suggesting a power law or Ostwald / de Waele model, [22, 71], as often applied for the rheology of colloids. The analysis of the data in terms of the power law model will also be discussed in the next chapter.

Also obtained from frequency sweep are the change in G' and G'' with angular frequency, illustrated in Figure 5.13. Both moduli for the ink containing 1.5 g of powder decrease with an increase in angular frequency, whereas for all the other inks there is an increase with an increase in frequency.

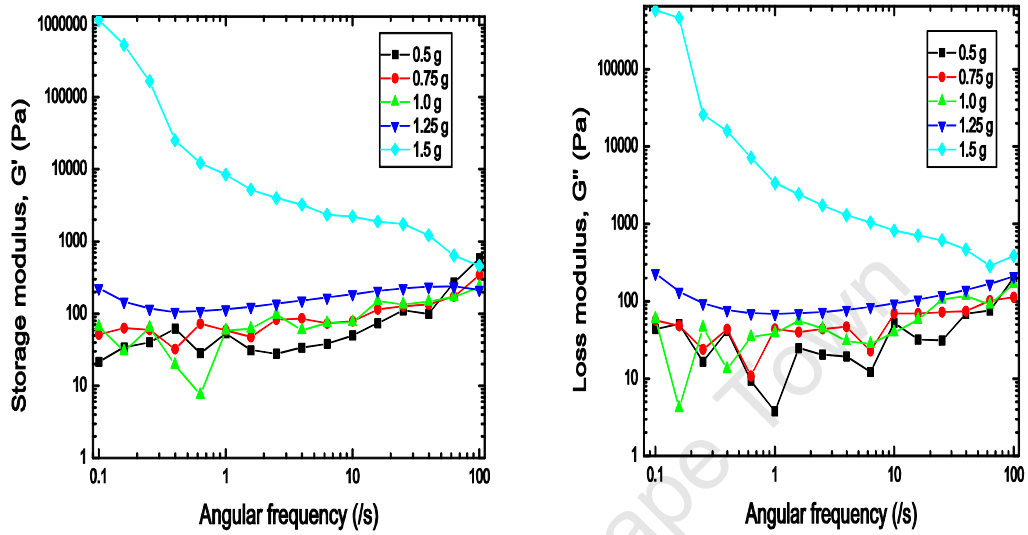

(a) (b)

Figure 5.13. (a) The storage modulus (G') and (b) loss modulus (G'') plot of silicon nanoparticle inks containing different particle loading.

The values of G'' are plotted against the values G' for all the inks in Figure 5.13, in an analogous manner to a Cole-Cole plot [93, 94]. The data is scattered around the middle line indicating that the inks have both viscous and elastic characteristics.

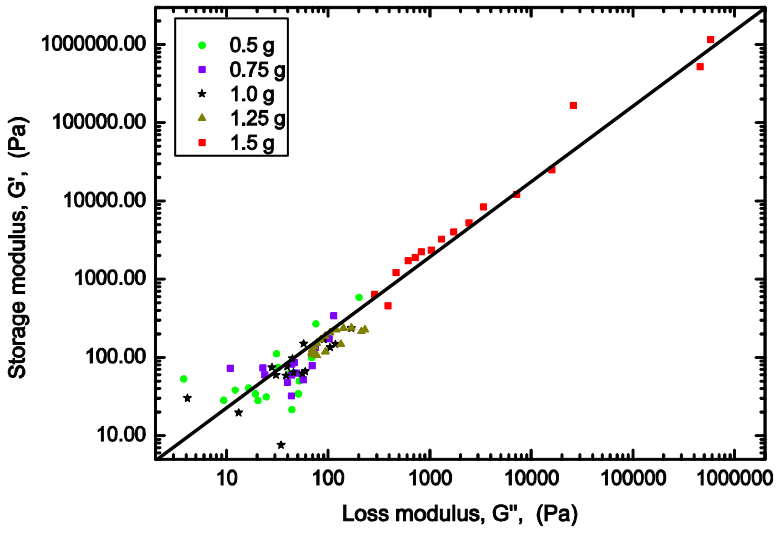

Figure 5.14. The graphs of G' vs G'' for inks with different particle loading.

Figure 5.15 represents the thixotropic measurements of silicon nanoparticle inks with different particle loading. As with the inks containing different amounts of solvent, the complex viscosity increases after deformation to a value that is higher than the original complex viscosity at rest. The viscosity for all the inks decreases when the inks are subjected to low shear rates before deformation. The ratio of $\eta^*_{(0)}$ to $\eta^*_{(1100s)}$ increases with an increase in particle loading, i.e. as the particle loading increases, the inks become more thicker with time after deformation. The time it takes for the complex viscosity to reach its original value, is approximately 300s for all the inks except at very high particle loading, i.e. Figure 5.15 e.

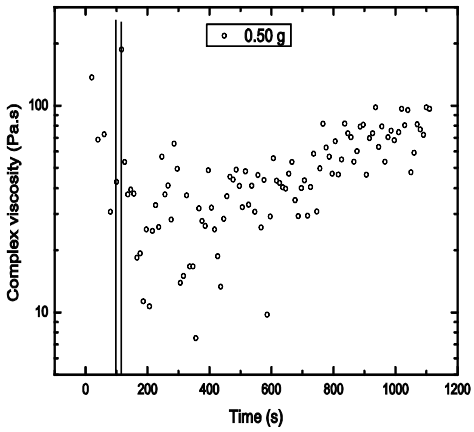

(a)

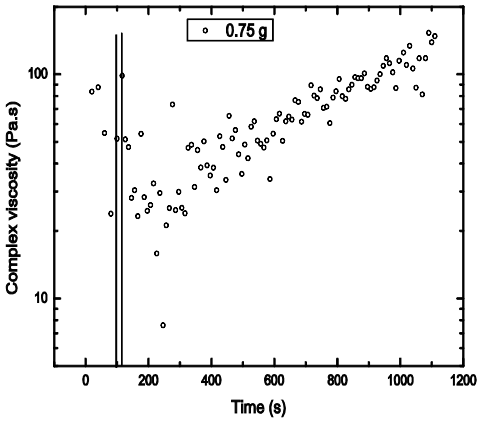

(b)

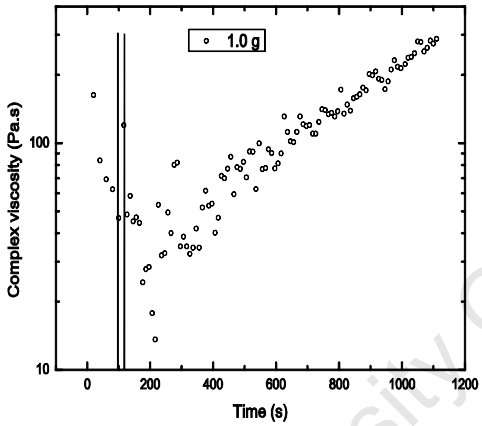

(c)

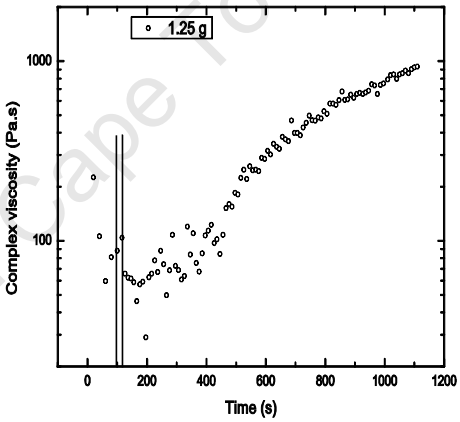

(d)

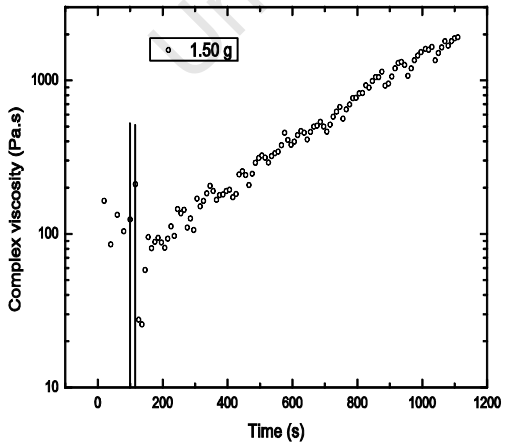

(e)

Figure 5.15. The thixotropy results of the complex viscosity curves for the ink containing different amounts of particle loading, where (a) 0.5. g, (b) 0.75 g, (c) 1.0 g, (d) 1.25 g and (e) 1.5 g of powder.

Contact angle measurements

The contact angles of silicon nanoparticle inks containing different amounts of particles were measured, as explained in section 4.1.2. The images of the droplets for the inks are presented in Figure 5.16 and the measured contact angle values are plotted as a function of particle loading in Figure 5.17.

The shape and size of the droplets change as the particle loading is increased. The higher the particle loading, i.e. image (e), the higher the contact angle the droplet makes with the surface. This could be accounted for by the increase in viscosity with particle loading that was seen in Figure 5.12. The colour of the droplets change from light brown to dark brown as the particle loading is increased.

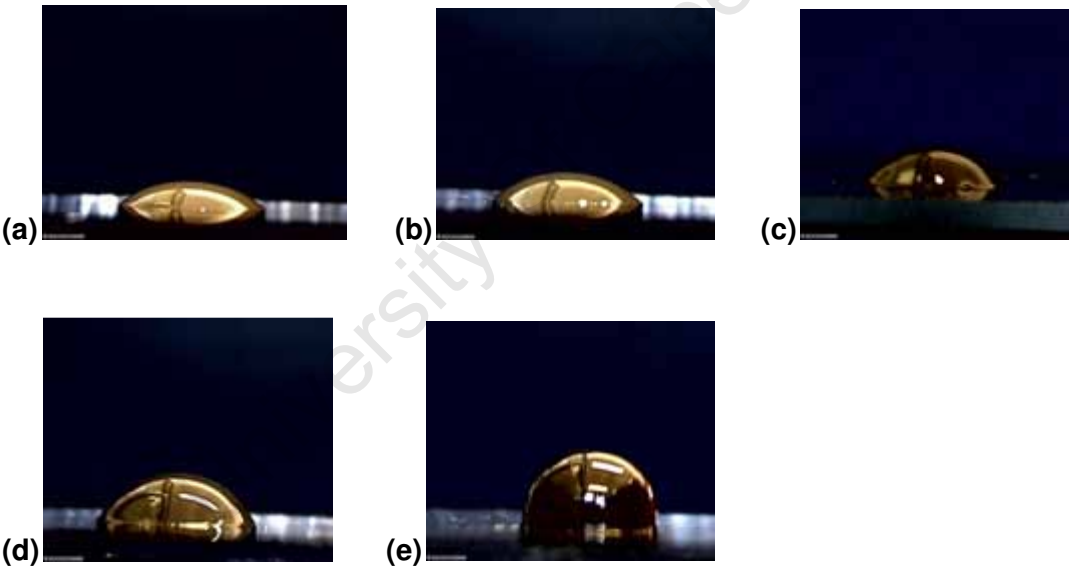

Figure 5.16. The images above are of the I-Si inks with different particle loading, (a) is 0.5 g, (b) 0.75 g, (c) 1.0 g, (d) 1.25 g, and (e) is 1.50 g of silicon nanoparticle powder.

In Figure 5.17, the contact angle of the droplet is seen to increase approximately exponentially as the particle loading is increased. The errors for the individual points are small compared to the size of the symbols.

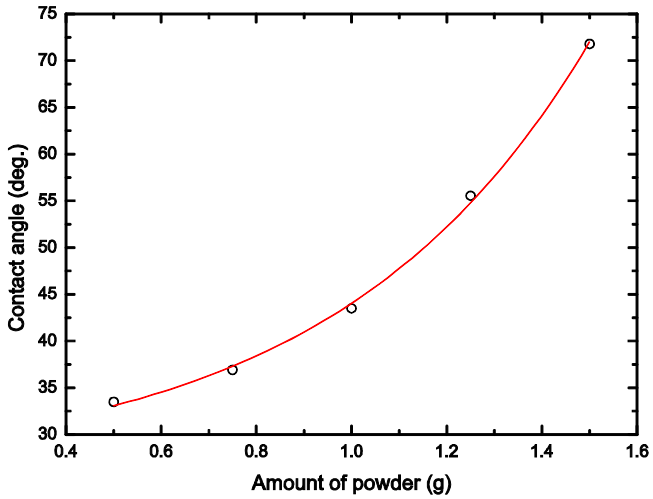

Figure 5.17. The contact angle of the inks with a glass slide as substrate, as a function of the amount of silicon nanoparticle powder added to the mixture.

5.2. PRINTED SILICON NANOPARTICLE LAYERS

The silicon nanoparticle inks were screen printed immediately after preparation, using the printing procedure outlined in section 4.3. The behaviour and appearance of the inks in the bowl and during the screen printing process is summarized in tables 5.3 and 5.4. The qualitative behaviour of the inks varied substantially, with inks containing low amounts of solvent drying on the screen and those with high amounts of solvent bleeding into the paper substrates.

Table 5.3. The appearance and behaviour of the inks before and after printing, where the amount of solvent is varied.

Amount of solvent (µL)	Appearance in bowl	Performance during printing	Printed layer	Overall impression
1500	Thick, pasty, high viscosity	Dries fast	Visible pin-holes	Not good for screen printing
1750	Pasty, but flows in the bowl	Print adequately	Good prints	Prints well but still dries fast
2000	Pasty and flows	Prints well	Good prints	Good consistency for printing
2250	Low viscosity	Prints well	Good prints	Good consistency for printing
2500	Very low viscosity	Easy to print	Ink bleeds	Viscosity is too low for printing

Variation of particle loading, shown in table 5.4, results in a different qualitative behaviour during the printing process. Inks containing high particle loads were generally thick and did not print well. However, for a wide range of particle loadings, covering a range of apparent viscosities, inks with a good printability could be achieved. It is, of course, not yet clear whether all these will be functional inks with good electronic properties when dry.

Table 5.4. The appearance and behaviour of the inks before and after printing, where the amount of particle loading is varied.

Amount of powder (g)	Appearance in bowl	Performance during printing	Printed layer	Overall impression
0.5	Low viscosity	Bleeds onto the substrate	Wets the substrate	Not good for screen printing
0.75	Low viscosity	Printed adequately	Good prints	Good consistency for printing
1.0	Pasty and flows	Prints well	Good prints	Good consistency for printing
1.25	High viscosity, paste-like	Prints adequately, dries fast	Good prints	Good ink for printing
1.50	Very high viscosity	Does not print well, blocks the screen	Very few good prints	Not good for printing

The printed layers were analyzed using scanning electron and optical microscopy, as detailed in section 4.4.1. The images that were taken using the optical microscope are presented in Figure 5.18 and Figure 5.19. For all the samples the magnification was 16X. The images shown in Figure 5.18 are optical micrographs of printed silicon nanoparticle layers, using inks containing different amounts of solvent on paper substrates.

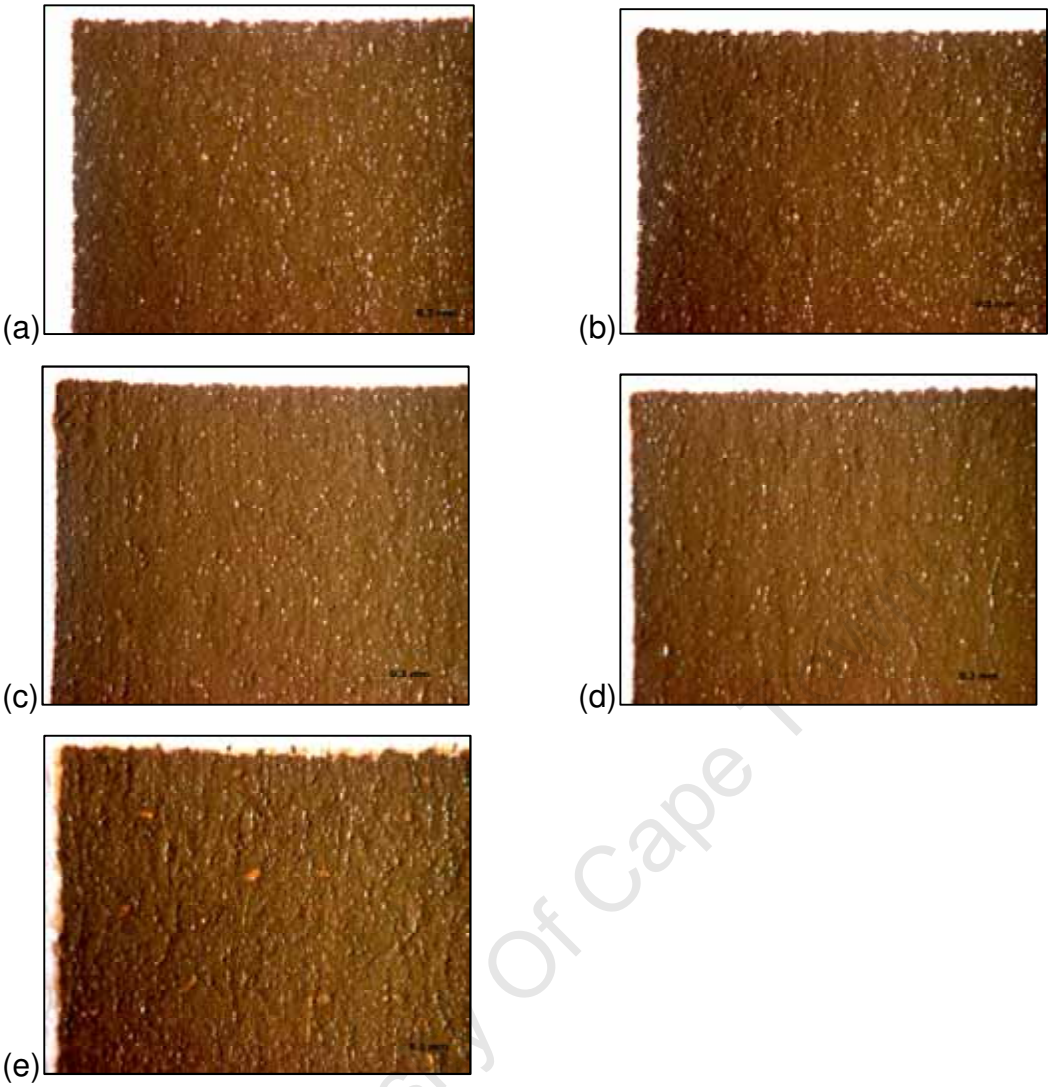

Figure 5.18. Optical microscope images of the printed silicon nanoparticle layers containing different amounts of solvent, where (a) 1500 µL, (b) 1750 µL, (c) 2000 µL, (d) 2250 µL and (e) 2500 µL.

The inks containing low amounts of solvent, i.e. images (a) and (b), have rougher edges and contain pinholes. These features are not seen in the Figure 5.18 (e), which used a high amount of solvent, where instead the edges have two colours. This characteristic could be attributed to the ink bleeding into the substrate.

The images in Figure 5.19 represent the printed layers of the inks with different particle loading.

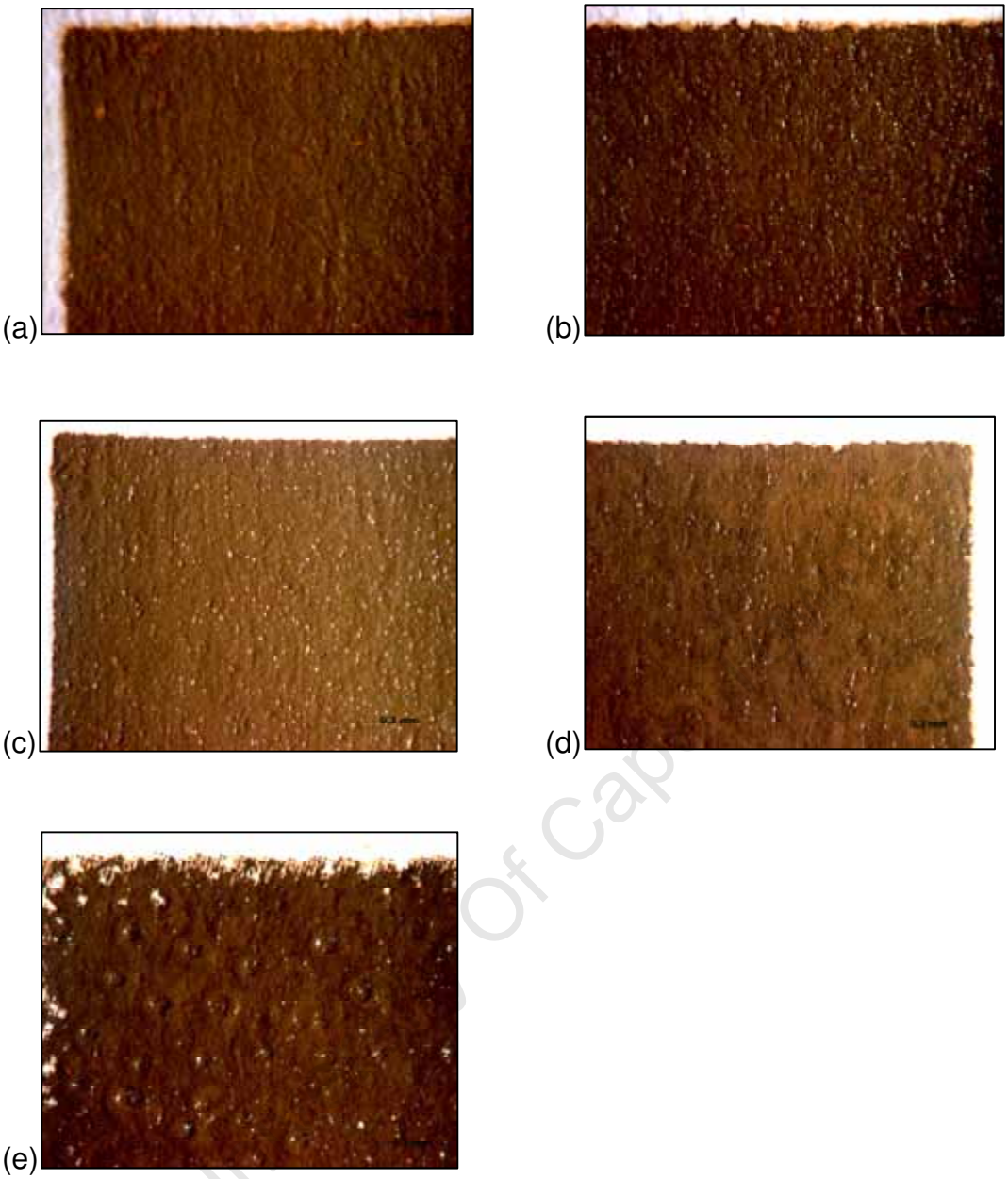

Figure 5.19. The optical microscope images of the printed silicon nanoparticle layers containing different amounts of particles, where (a) 0.50 g, (b) 0.75 g, (c) 1.0 g, (d) 1.25 g and (e) 1.50 g.

The images for the inks containing low amounts of powder, i.e. images (a) and (b), have edges that show two colours and are more uneven than the other inks. This could be because of the inks bleeding into the substrate during the drying process. In contrast, the layer printed with the ink containing a high amount of powder, image (e), contained large pinholes and showed very poor edge definition.

SEM images were taken to investigate the morphology of the samples and the cross-sectional view of the printed layers for all the 9 inks prepared.

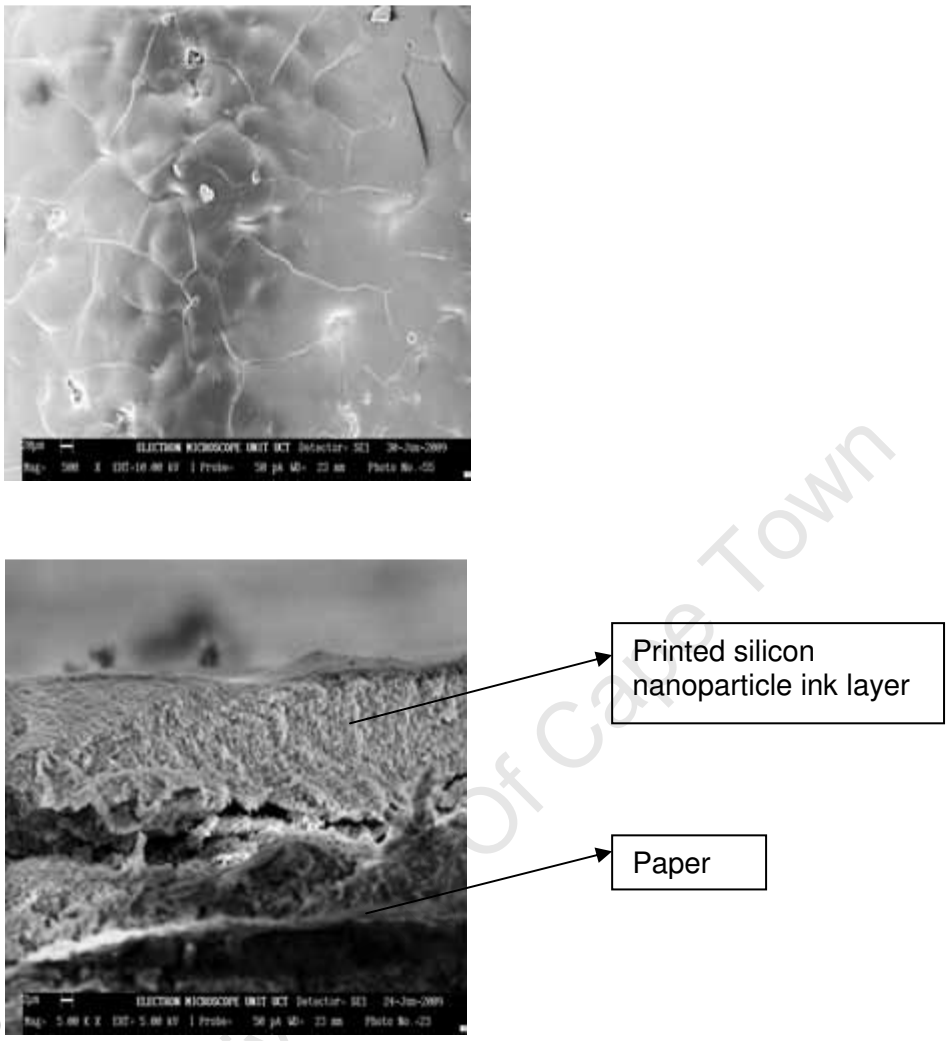

Figure 5.20. Scanning Electron Microscope images of printed layers, (a) the surface and (b) cross-section.

The two images in Figure 5.20 are representative of the printed silicon nanoparticle inks. The layers showed signs of microscopic surface cracking after air drying for 24 hours, (Figure 5.20a). This was present in all the inks containing different amounts of powder and solvent. The cross-section of the printed layers shows a solid and compact structure. The horizontal crack visible in Figure 5.20b is an artifact of the sample cutting and indicates low mechanical strength of the printed layer and not poor adhesion to the substrate.

5.3. ELECTRICAL CHARACTERIZATION

5.3.1. Resistance measurements

According to the description given in Chapter 4, the silicon nanoparticle inks containing different amounts of solvent and particle loading were screen printed onto paper substrates. The inks were printed as resistors whose resistance was measured using the Keithley 4200-CSC semiconductor characterization system as explained in section 4.4 in order to determine the electrical performance of the inks. The resistance of inks containing different amounts of solvent is plotted in Figure 5.21, where each data point is an average of 10 measurements of different resistor samples from the same ink with the error bars determined using standard uncertainty methods.

The resistance of the ink increases with the amount of solvent added, reaching a maximum of about 1.5 $G\Omega$ for the ink containing 2000 µL of solvent and remaining constant for further dilution.

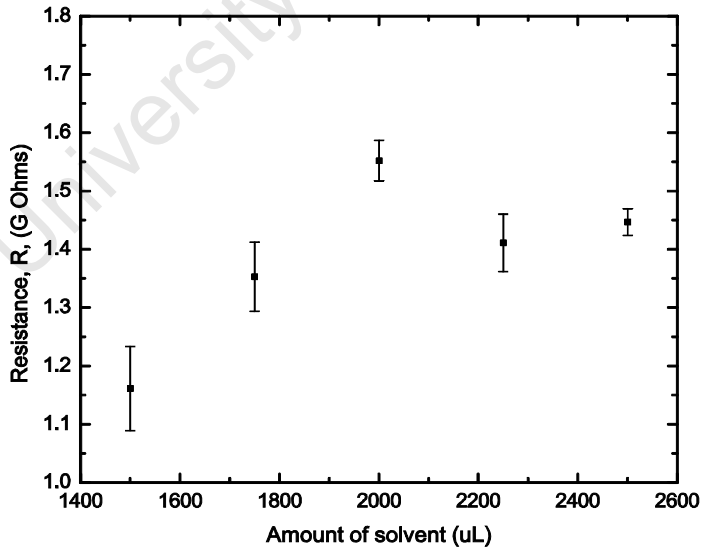

Figure 5.21. The resistance measurements of the inks that contain different amounts of solvent.

The resistances of the inks containing different amounts of powder are plotted in Figure 5.22; with the error bars calculated using standard uncertainty methods. As with the ink containing different amounts of solvent, the resistance plotted here is an average of 10 measurements per ink. The resistance of the printed layers remains constant as the particle loading is increased, only increasing for the sample containing 1.50 g of powder.

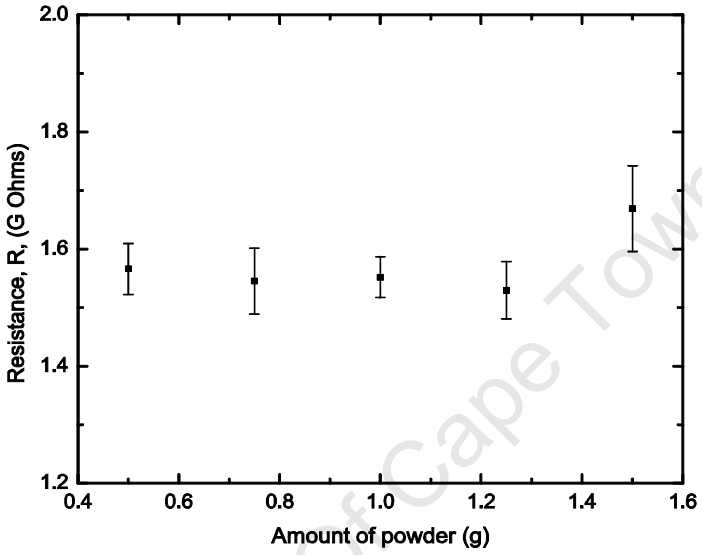

Figure 5.22. The resistance measurements of the inks containing different amounts of powder.

5.3.2. Photo-response of the printed layers

The current and voltage response of the printed electronic devices with the silicon nanoparticle ink containing 2000 µL of solvent as the active layer are represented in Figure 5.23. The ink was screen printed on top of a silver layer and with a transparent conductor as the top layer.

The voltage measurements were started with the light switched off for 300 s, under which conditions the measured potential was 240 µV. As the light was switched on, the voltage decreased sharply to 70 µV for 300s and increased again when the light was switched on.

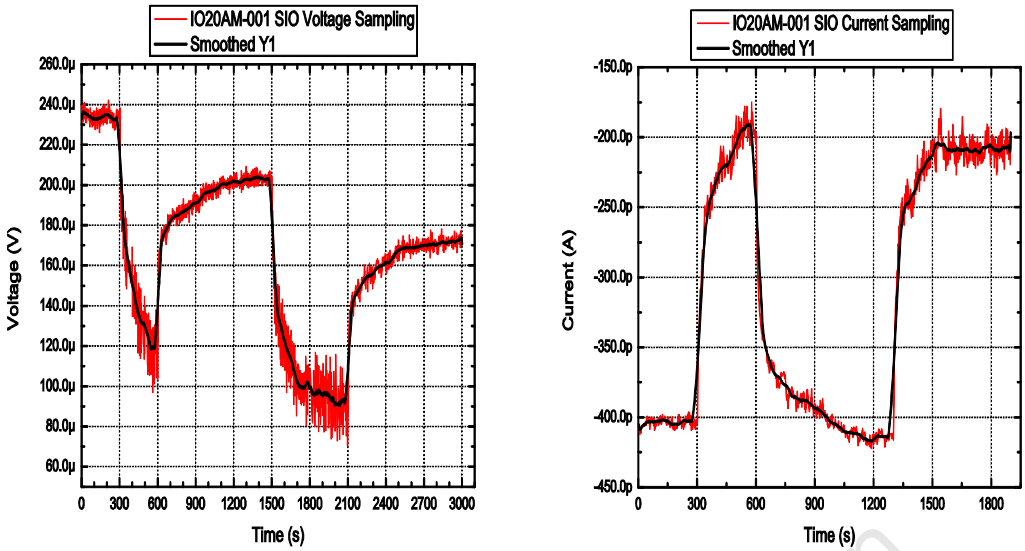

(a) **(b)**

Figure 5.23. The graphs of voltage current and output for the single layers of I-S between two contacts.

For the current response, the dark current was initially -400 pA and increased rapidly to a maximum of -200 pA when the light was switched on for 300s. After the light was switched off again, the current decreased until it reached a level of -420 pA.

CHAPTER 6: DISCUSSION

6. DISCUSSION

6.1. INK PROPERTIES

6.1.1. Rheology

For the inks containing different amounts of solvent, the storage and loss moduli both decrease as the amount of solvent added to the ink is increased, as shown in Figure 5.1. The inks become both less shear thinning and less viscous with an increase in the amount of solvent added. This is due to the particles being more dispersed in the ink as the amount of solvent is increased, therefore lowering the strength of inter-particle interactions which contribute to the high viscosity of the inks [24].

In the linear viscoelastic range the storage modulus dominates over the loss modulus, making the material more elastic than viscous. After severe deformation the opposite occurs and the material becomes more viscous. The cross-over point which occurs at low strain values and decreases with the increase in the amount of solvent is known as the gel-point [22]. As the amount of solvent is increased and the particles become more dispersed, the gel point occurs at lower strain.

All the flow curves in Figure 5.2 show behaviour that is indicative of shear thinning materials, i.e. there is a decrease in slope with strain. As the amount of solvent added into the inks is increased, the shear strength of the inks decreases. The relationship between the shear stress and strain is similar to the Windhab model behaviour, discussed in 3.1.1 and table 3.2, and therefore the data was modeled accordingly as [22], using the Windhab model.

To use the Windhab equation for strain-shear stress relationship it can be re-written as:

$$\tau = \tau_0 + J_e.\gamma + (\tau_1 - \tau_0).\left[1 - \exp\left({}^{-\gamma}/_{\gamma^*}\right)\right], \qquad (6.1)$$

where τ = shear stress, τ_0= yield stress, τ_1= maximum shear-induced stress, γ= strain, γ^* is a constant and J_e is the reciprocal equilibrium shear compliance, which is equal to the characteristic shear stress-strain gradient.

Figure 6.1 shows the flow curves from Figure 5.2 fitted with the Windhab equation (equation 6.1) to determine the yield point and the maximum shear-induced stress of the material [22, 74].

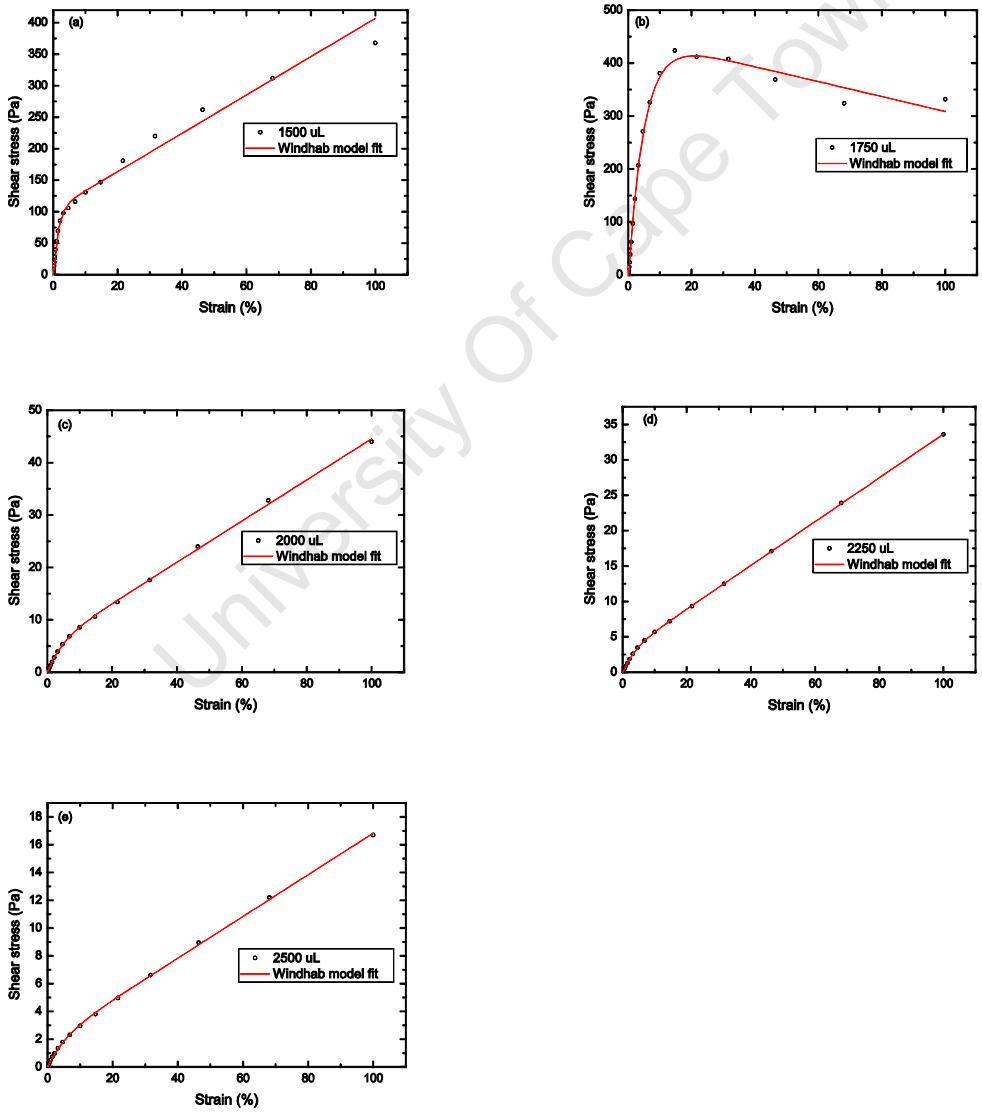

Figure 6.1. The fitted curves for flow curve data of the inks containing (a) 1500 µL, (b) 1750 µL (c) 2000 µL, (d) 2250 µL and (e) 2500 µL of solvent.

A good agreement is obtained for all the flow curves. Therefore it can be said that the flow of the silicon nanoparticle inks follows the Windhab model behaviour adapted to shear stress-strain relationship. The yield point and the maximum shear induced stress decreases as the amount of solvent is increased and the silicon nanoparticles in the ink become more dispersed (see table 6.1). The yield stress of the ink containing 1750 µL of solvent is very high compared to that of the other inks which, was seen qualitatively in Figure 5.2 when the curves were plotted on the same axis.

Table 6.1. The results of the Windhab model fitted flow curves of the inks containing different amounts of solvent.

Amount of solvent (µL)	Yield stress, τ_0, (Pa)	Max. shear induced stress, τ_1, (Pa)
1500	0.0092	103.1
1750	7.89	440.8
2000	0.035	5.29
2250	0.034	2.75
2500	0.021	1.84

The main information obtained from the frequency sweep is the change in complex viscosity with angular frequency shown in Figure 5.3. The viscosity decrease as the amount of solvent added into the ink is increased. For each individual ink the viscosity decreases with an increase in angular frequency indicating shear thinning behaviour. The inks have similar viscosity values at higher frequencies, making high frequency viscosity measurements, e.g. as measured with a viscosimeter, unreliable. In dispersions, shearing can cause the particles to orient in the flow direction and in the direction of shear gradient [42]. Shearing can also cause agglomerates to disintegrate or particles to change their form [63]. During this process, the interaction forces between the particles usually decrease and this lowers the viscosity.

For the inks containing high solvent amounts, the logarithmic decrease in complex viscosity, η^*, with logarithm of angular frequency, ω, is linear which suggested that the data will fit a power law model, discussed in detail in section 3.1.3,

$$\eta^* = K\omega^n \ , \qquad (6.2)$$

where K is a constant and n is a power law index.

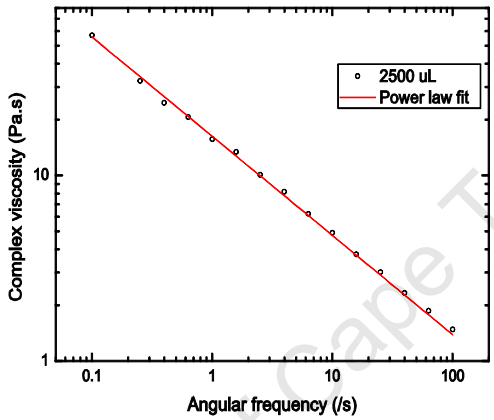

Figure 6.2 a. The Power law model of silicon nanoparticle ink containing 2500 µL solvent.

A simple power law model only describes the highly dispersed and dilute ink that contains 2500 µL of solvent. The data for highly concentrated inks can be fitted with a combined power law. The data for the ink containing 1500 µL and 2250 µL of solvent were fitted with equation 6.3 to form a combined power law because the curves have two distinct areas of linearity. Using this model, the power law index at high frequency for all the inks is given in table 6.2.

$$\eta^* = K_1\omega^{n_1} + K_2\omega^{n_2} \ . \qquad (6.3)$$

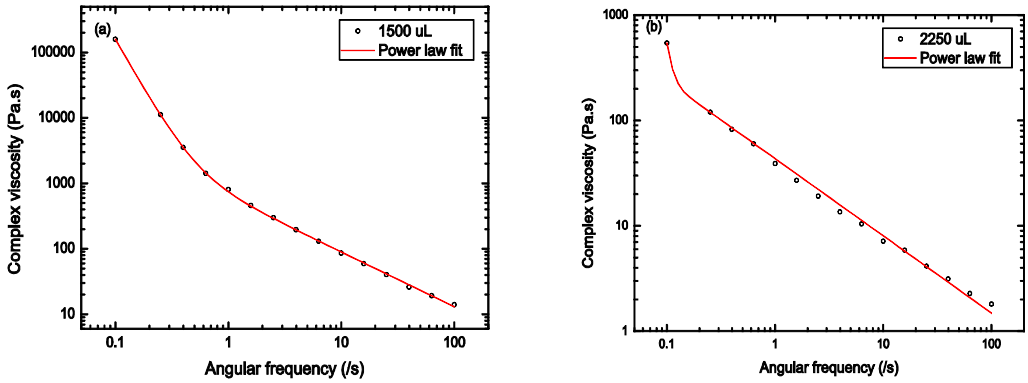

Figure 6.2 b. The power law model of silicon nanoparticle inks with different amounts of solvent, (a) 1500 µL (b) 2250 µL.

Table 6.2. The values of the power law index for the inks containing different amounts of solvent

Amount of solvent (µL)	High frequency Power law index ($\|n\|$)
1500	0.79
2250	0.67
2500	0.55

The high frequency limit, n_2, is used from the combined power law because it represents the behaviour of the inks at high shear rates and provides the longest range of linearity. As the amount of solvent in the ink is increased, the power law index decreases. The shear thinning range is: $0 < n < 1$ and the closer the value is to 1, the more shear thinning the material [46, 70]. The more dilute the ink, the less shear thinning the material.

The remaining frequency sweep data is represented by Figure 5.4, which shows the frequency dependence of the storage and loss moduli for inks that contain different amounts of solvent. As with the amplitude sweep data, both storage and loss moduli values decrease with the increase in the amount of solvent because the solvent causes the particles to become dispersed in the colloid. Storage dominates over loss for all the inks at low frequencies but there is a cross-over point where the loss modulus dominates over the

storage modulus at higher frequencies. This suggests that the inks not only have viscous short-term behaviour and elastic long-term behaviour, but that after extended time in storage the inks will harden, i.e. become more elastic [22].

From the thixotropy data (Figure 5.14) the viscosity after deformation increases to a value that is larger than the original static viscosity. This could be due to solvent evaporation during high shear (deformation) stage of the measurement. This shear thickening behaviour normally occurs after a period of shear thinning [95]. Hoffman [24, 96] accounts shear thickening to the transition from an ordered to a disordered state of the material. The higher the amount of solvent in the ink, the longer it takes for the ink structure to recover after deformation. The ink with high solvent loading (Figure 5.14 d) is dilute and has less particle-particle interactions leading to a longer time-lag for the structural recovery compared to inks containing low amounts of solvent, which have higher particle-particle interactions. This is also seen in the difference between $\eta^*_{(0)}$ and $\eta^*_{(1100s)}$ which decreases as the amount of solvent in the inks is increased.

When the particle loading of the ink is varied there is a trend in the amplitude sweep data, where storage and loss moduli increase with an increase in the amount of particle loading (Figure 5.9). For all the inks the storage and loss moduli both show a decrease after the LVE range meaning that the inks are shear thinning. Shear thinning is due to a distortion of the liquid-like structure which then leads to a decrease in energy dissipation, G' < G'' [42]. There is a cross-over point that was observed for all the samples. The strain at which this point occurs increases with an increase in the particle loading suggesting that, as the viscosity of the inks increase the strain necessary for the inks to start flowing increases. After the cross-over point, the loss modulus dominates over the storage modulus, making the inks more viscous and less elastic as the strain increases.

There is a large difference in the required shear stress between the sample containing 1.25g of powder and the sample containing 1.5 g of powder of approximately 10 in order of magnitude, shown in Figure 5.10. This suggests an intermediate structure in this range of particle loading. However, in general, the shear stress is higher for inks at higher particle loading and decreases as the particle loading decreases. The data for the stress vs. strain curves was fitted with the Windhab model (equation 6.1), to determine the yield point, as shown in Figure 6.3, and discussed in section 3.1.3.

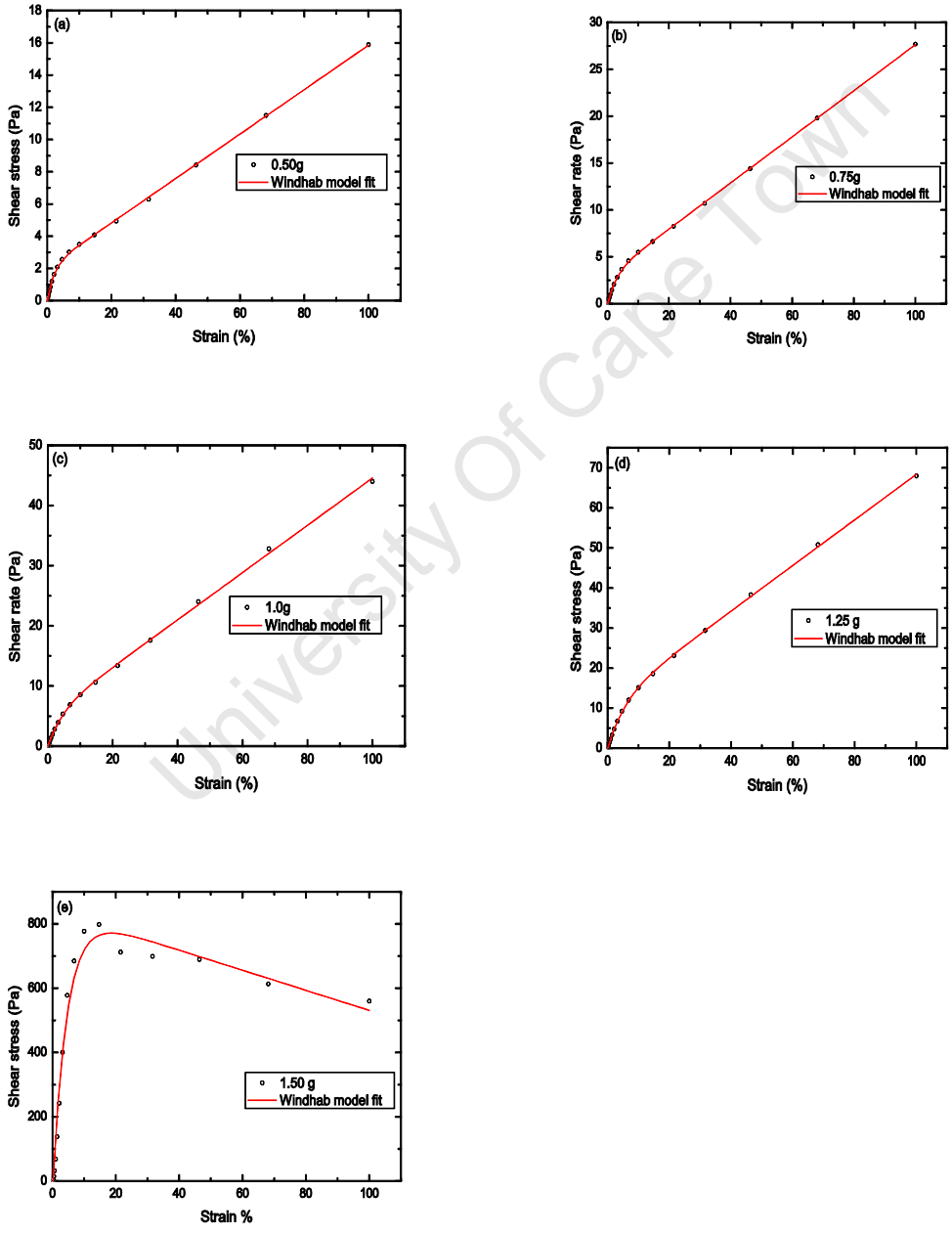

Figure 6.3. The fitted flow curves for the inks containing different amounts of silicon nanoparticle (a) 0.5 g, (b) 0.75 g, (c) 1.0 g, (d) 1.25 g, and (e) 1.50 g.

As for the inks with varied amounts of solvent, the data agree well with the Windhab model. This model determined not only the yield point but also the shear stress that leads to the maximum shear-induced structuring. The yield point and maximum shear-induced stress increase as the particle loading increases, as indicated in table 6.3. This increase in yield point as the particle loading is increased was also noticed by Luckham, et al for polystyrene dispersions [56].

Table 6.3. The results from the Windhab model fitted flow curves of the inks containing different amounts of particle loading.

Particle loading (g)	Yield stress, τ_0, (Pa)	Max. shear induced stress, τ_1, (Pa)
0.50	0.034	2.07
0.75	0.049	3.04
1.0	0.034	5.31
1.25	0.048	11.44
1.50	35.10	843.20

The complex viscosity (Figure 5.11) decreases as the angular frequency increases which is indicative of shear thinning fluids. The higher the particle loading, the higher the viscosity value and the inks with higher particle loading show more shear thinning. The inks have similar viscosity values at higher frequencies making the high frequency viscosity measurements of the inks unreliable. The dependence of the complex viscosity on angular frequency does not exhibit an obvious power law, except for the ink containing 1.25g of powder at high frequencies. The complex viscosity data of this ink was fitted with the combined power law model (equation 6.3) as shown in Figure 6.4. The value of the power law index (n_2) obtained from fitting the data is 0.79, which is in the shear thinning range (section 3.13) [46].

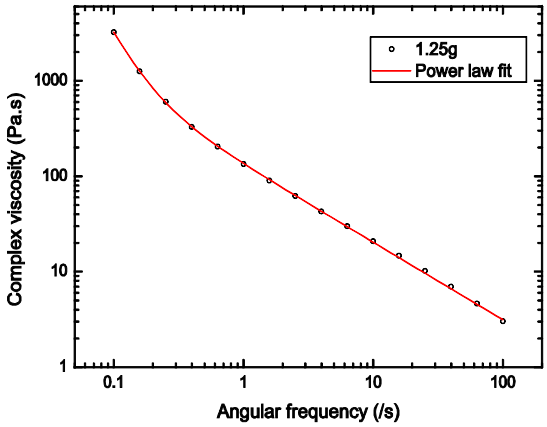

Figure 6.4. The power law fitting for the complex viscosity data of the ink containing 1.25 g powder.

The storage and loss moduli for the inks containing 1.25 g of powder and less show an increase with the increase in angular frequency, whereas inks containing 1.5 g of powder show a decrease with an increase in angular frequency. The storage modulus dominates over the loss modulus for low frequency and there is a cross-over point after which loss modulus dominates over storage modulus, implying that the inks have viscous short-term behaviour and elastic long-term behaviour.

The solvent evaporates as the inks are subjected to high shear rates which lead to an increase in viscosity after deformation from the thixotropy measurements (see Figure 5.15). All the inks contain the same amount of solvent and the difference between $\eta^*_{(0)}$ and $\eta^*_{(1100s)}$ is much smaller than that seen for inks containing different amounts of solvent. The higher the particle loading in the ink, the shorter the time it takes for the inks to recover after deformation. The same argument used for the solvent variation applies, in that the inks that are highly viscous and concentrated have more particle-particle interactions and thus exhibit faster recovery. Lin, et al, found that this thixotropy behaviour is more pronounced in pastes containing high concentrations of particles [4]. This is the same behaviour seen in Figure 5.14 suggesting that the highly viscous inks have more stable structures.

6.1.2. Surface Properties of Silicon Nanoparticle Inks

For inks with varied amount of solvent (Figure 5.8) as the amount of solvent is increased, the contact angle decreases. The decrease in contact angle with an increase in solvent is an S-shaped decline curve saturating at high amounts of solvent. The change in contact angle with solvent could be accounted to the fact that contact angle is a consequence of inter-particle or intermolecular interactions [3, 9]. Spreading and wetting of a surface by a fluid arise from the intermolecular forces of the fluid [3, 42]. Also, the higher the particle-particle interaction of the ink, the less likely the ink will spread or wet the substrate [42], resulting in a higher contact angle. The increase in solvent decreases the particle-particle interactions, [24], and therefore the contact angle of the fluid will decrease, making it easier to spread and wet the surface.

For inks with varied particle loading, the higher the particle loading, the higher the contact angle. The increase of contact angle in relation to the particle loading is an exponentially increasing curve, shown in Figure 5.15. The higher the particle loading in the ink, the higher the particle-particle interactions and therefore the higher the contact angle. When the interfacial tension of the ink is higher than that of the ink with the substrate, the ink will not spread or wet the surface [9, 42].

This change in contact angle with the amount of solvent and particle loading correlates to the rheological measurements, which showed that the shear strength of the ink depends on the particle-particle interaction. The higher the particle loading, the higher the shear strength and the contact angle, i.e. the more viscous inks have higher particle-particle interactions.

6.2. PRINTABILITY

Tables 5.3 and 5.4 outlines the behaviour of the inks during printing. As the amount of solvent added into the inks is increased the printability of the inks improves giving better printed structures, but at very high solvent loading the inks bleed onto the paper substrate. With the change in particle loading, as the particle loading is increased, the inks dry on the screen and are difficult to print. For both the solvent and particle loading varied inks, the more viscous the ink, the higher the contact angle and the harder it is to print. Therefore the printability of the inks can be related to the surface tension of the ink, where the higher the surface tension, the more difficult it is to print the ink [3]. Ideally, the surface tension of the ink should be small, with a small contact angle, so that the ink can be able to spread onto the substrate with ease [3].

Optical microscope and SEM images in Figure 5.16 - 5.17 and Figure 5.18 respectively, show the morphology of the printed layers. The SEM images show a compact layer with microscopic cracks which formed during drying. The nanoparticle structure cannot be seen properly because of the size of the particles and the compactness of the particles in the ink [92]. The optical microscope images show that the layers have a rough, compact structure with the ink containing the highest amount of particles exhibiting large pinholes and badly printed edges. This is in agreement with the analysis that the higher the particle loading, the higher the surface tension from the particle-particle interaction and therefore the harder it is to print the ink resulting in a structure with pinholes.

6.3. ELECTRICAL CHARACTERIZATION

The resistance of the printed silicon nanoparticle layers changes with both the amount of solvent and particle loading, see Figures 5.19 and 5.20 respectively. As the amount of solvent added is increased, the resistance increases to a maximum and then decreases to a constant value with more solvent added. However, as the particle loading is increased, the resistance remains constant and only increases at the highest particle loading. There is however no clear trend in the change in resistance of the printed layers with the composition of the inks. Well printed layers are important in order to obtain a network structure of the printed nanoparticles because inks with high surface tension were hard to print and this resulted in badly printed devices with large pinholes that will cause a short circuit.

The printed layers showed electro-optical activity measured by their voltage and current response to a fluorescent light, in Figure 5.21 [92]. The voltage decreases when the light is switched on and current increases when the light is switched on. Therefore it can be concluded that the printed silicon nanoparticle layers show optical activity. However, since only one ink was measured for photoresponse, the relationship between ink properties and electrical activity cannot be properly established.

CHAPTER 7: CONCLUSION

7. CONCLUSION

The primary aim of this project was to determine the rheological behaviour of silicon nanoparticle inks used for screen printing electronic devices. The inks were prepared using different amounts of solvent and particle loading to determine the effect that changing these parameters will have on the properties of the inks. Specific rheological properties, i.e. storage and loss moduli, shear stress required for flow and viscosity, increase as the particle loading is increased and decrease as the amount of solvent is increased. Shear thinning behaviour is the main requirement for screen printing and rheological characterization showed that all the inks are shear thinning as well as being partially thixotropic and viscoelastic.

The flow behaviour of the inks was observed to follow the Windhab model. It was also discovered that at certain solvent and particle loading, a simple and a combined power law (Ostwald / de Waele model) could be used to describe the angular frequency-dependent viscosity behaviour of the inks. The higher the concentration of solid matter in comparison to liquid component, the higher the viscosity and required stress and the harder it is to obtain good printed layers, thus affecting the electrical properties of the finished device.

The ultimate purpose of this project was to establish a relationship between the properties of the ink, the structure of printed layer and its electrical activity. A relationship between the rheology and the surface properties of the ink, to its printability has been successfully developed. This relationship can simply be expressed as that the more viscous the ink, the higher the surface tension and the poorer the printability. For complex viscosities above 6 Pa.s, high contact angles are observed and printability is poor with regard to uniformity. Similarly below 2 Pa.s, low contact angles are observed and leads to ink bleeding. From a technical point of view, a defined range for the contact angle could be established which allows us to evaluate the printability of the ink,

which leads in printed nanoparticulate silicon to satisfy electronic response. Though more work needs to be done with regard to electrical characterization of printed devices, this research has also managed to successfully screen-print silicon nanoparticle inks in electronic devices and fulfilled the basic requirement of producing a continuous network of particles to allow electrical conduction [97].

Understanding the full rheological behaviour of all the inks used has already enabled the production of screen printable inks that result in good electrical properties of the semiconductor layer. For future work, the rheological findings in this work will be used as a benchmark for determining the behaviour of inks prepared with different types of silicon nanoparticles. The ink preparation procedure will be optimised to obtain uniform inks. The thixotropy measurements need to be further developed, as fully thixotropic inks are required for optimal screen printing.

REFERENCES

[1] A. Griffiths, Prints and printmaking : An introduction to the history and techniques British Museum Press, Avon, 1996.

[2] J. Heller, Printmaking today : A studio handbook, Holt, Rinehart and Winston, New York, 1972.

[3] K. E. G. Pitt, Handbook of Thick Film Technology, Electrochemical Publications Limited, Port Erin, British Isles, 2005.

[4] H.-W. Lin, C.-P. Chang, W.-H. Hwu, and M.-D. Ger, Journal of Materials Processing Technology 197 (2008) 284

[5] A. Kosloff, Screen Printing Electronic Circuits, Times Publishing, 1980.

[6] A. Sanson, D. Gardini, G. Montanari, C. Galassi, and E. Roncari, Journal of Materials Research 21 (2006) 1561

[7] T. E. Karis, Journal of Applied Polymer Science 59 (1996) 1405

[8] T. Young, Philosophical Transactions of the Royal Society of London 95 (1805) 65

[9] C. Vladuta, L. Andronic, M. Visa, and A. Duta, Surface and Coating Technology doi:10.1016/j.surfcoat.2007.08.033 (2007)

[10] W. M. Ivins, How Prints Look : Photographs with Commentary, Beacon Press, Boston, 1987.

[11] H. Ezawa, M. Seto, M. Miyata, and H. Tazawa, Microelectronics Reliability 43 (2003) 473

[12] J. H. Cho, J. Lee, Y. Xia, B. Kim, Y. He, M. J. Renn, T. P. Lodge, and C. D. Frisbie, Nature Materials 7 (2008) 900

[13] D. T. Britton, in Plastic Electronics Asia, China, 2008.

[14] M. Lahti, S. Leppavuori, and V. Lantto, Applied Surface Science 142 (1999) 367

[15] T. Makela, T. Haatainen, P. Majander, and J. Ahopelto, Microelectronic Engineering 84 (2007) 877

[16] A. Kosloff, Screen printing techniques, The Sign of the Times Publishing, 1981.

[17] C. Weisbecker, R. Durand, and G. Pace, Chemometrics and Intelligent Laboratory Systems 93 (2008) 20

[18] M. L. Chabinyc, W. S. Wong, A. C. Arias, S. Ready, R. A. Lujan, J. H. Daniel, B. Krusor, R. B. Apte, A. Salleo, and R. A. Street, Proceesings of the IEEE 93 (2005) 1491

[19] F. Menil, H. Debeda, and C. Lucat, Journal of the European Ceramic Society 25 (2005) 2105

[20] S. Turner, Screen printing techniques, Taplinger Publishing Co., Inc, New York, 1979.

[21] V. Bonvicini, M. Caccia, P. Mazzoni, C. Napoletano, M. Pindo, N. Redaelli, A. Samori, and G.Vegni, Nuclear Physics B (Proc. Suppl.) 44 (1995) 409

[22] T. G. Mezger, The Rheology Handbook, Vincentz, Hannover, 2002.

[23] P. S. a. Marcos, J. Marto, T. Trindade, and J. A. Labrincha, Journal of Photochemistry and Photobiology A: Chemistry 187 (2007) 125

[24] A. Zupancic, Journal of European Ceramic Society 18 (1998) 467

[25] R. Mannerbro, M. Ranlof, N. Robinson, and R. Forchheimer, Synthetic Metals 158 (2008) 556–560.

[26] R. Parashkov, E. Becker, T. Riedl, H.-H. Johannes, and W. Kowalsky, Proceesings of the IEEE 93 (2005) 1321

[27] H. C. Jung, S.-H. Cho, J. W. Joung, and Y.-S. Oh, Journal of Electronic Materials 36 (2009) 1211

[28] P. Beecher, P. Servati, A. Rozhin, A. Colli, V. Scardaci, S. Pisana, T. Hasan, A. J. Flewitt, J. Robertson, and G. W. Hsieh, Journal of Applied Physics 102 (2007) 043710.

[29] J. Shan, P. Pulkkinen, U. Vainio, J. Maijala, J. Merta, H. Jiang, R. Serimaa, E. Kauppinen, and H. Tenhu, Journal of Materials Chemistry 18 (2008) 3200

[30] A. J. Lennon, R. Y. Utama, M. A. T. Lenio, A. W. Y. Ho-Baillie, N. B. Kuepper, and S. R. Wenham, Solar Energy Materials and Solar Cells 92 (2008) 1410

[31] V. Sanchez-Romaguera, M.-B. Madec, and S. G. Yeates, Reactive & Functional Polymers 68 (2008) 1052

[32] E. K. Fischer, Colloidal dispersion, John Wiley & Sons, New York, 1950.

[33] H. Kippman, Handbook of Print Media, Springer, 2001.

[34] L. K. Branson, Introduction to Electronics, Prentice-Hall, New Jersey, 1967.

[35] J. M. Clavert and M. A. H. McCausland, Electronics, John Wiley & Sons, Chichester, 1978.

[36] U. Zschieschang, M. Halik, and H. Klauk, Langmuir 24 (2008) 1665

[37] G. Gruner, Journal of Materials Chemistry 16 (2006) 3533

[38] H. Buckingham and E. M. Price, Principles of Electronics, Cleaver-Hume Press Ltd, London, 1958.

[39] J.-H. Ahn, H.-S. Kim, K. J. Lee, S. Jeon, S. J. Kang, Y. sun, R. G. Nuzzo, and J. A. Rogers, Science 314 (2006) 1754

[40] M.-Y. Choi, Y. Kim, and C.-S. Ha, Progress in Polymer Science 33 (2008) 581

[41] J. R. Van Wazer, J. W. Lyons, K. Y. Kim, and R. E. Colwell, Viscosity and flow measurement : A Laboratory Handbook of Rheology, Interscience Publishers, New York, 1963.

[42] D. J. Shaw, Introduction to colloid and surface chemistry, Butterworths, London, 1980.

[43] D. Bell, Physics Education 14 (1979) 432

[44] A. Dinsdale and F. Moore, Viscosity and its measurements, Chapman and Hall Limited, London, 1962.

[45] E. C. Bingham, Fluidity and Plasticity, McGraw-Hill Book Company, Inc, New York, 1922.

[46] M. J. Santillan, F. Membrives, N. Quaranta, and A. R. Boccaccini, Journal of Nanoparticle Research 10 (2008) 787

[47] P. Hahne, E. Hirth, I. E. Reis, K. Schwichtenberg, W. Richtering, F. M. Horn, and U. Eggenweiler, Solar Energy Materials and Solar Cells 65 (2001) 399

[48] T. Mezger, Vol. 2009, 1999.

[49] T. G. Mason, J. Bibette, and D. A. Weitz, Journal of Colloid and Interface Science 179 (1996) 439

[50] J. C. Baird and J. Y. Walz, Journal of Colloid and Interface Science 306 (2007) 411

[51] C. J. Brinker and G. W. Scherer, Sol-Gel Science : The Physics and Chemistry of Sol-Gel Processing, Academic Press, Inc., San Diego, 1990.

[52] E. F. Burton, The Physical Properties of Colloidal Solutions, Longmans, Green and Co., Toronto, 1938.

[53] W. B. Russel, D. A. Saville, and W. R. Schowalter, Colloidal dispersions, Cambridge University Press, Cambridge, 1989.

[54] H. R. Kruyt, Colloid Science, Elsevier Publishing Company, Amsterdam, 1952.

[55] Z. Adamczyk, B. Jachimska, and M. Kolansika, Journal of Colloid and Interface Science 273 (2004) 668

[56] P. F. Luckham and M. A. Ukeje, Journal of Colloid and Interface Science 220 (1999) 347

[57] M. D. Chadwick, J. W. Goodwin, B. Vincent, E. J. Lawson, and P. D. A. Mills, Colloids and Surfaces A: Physicochemical and Engineering Aspects 196 (2002) 235

[58] T. G. Mason and D. A. Weitz, Physical Review Letters 75 (1995) 2270

[59] J. Mewis, International Journal of Mineral Processing 44 - 45 (1996) 17

[60] K. Dullaert and J. Mewis, Journal of Colloid and Interface Science 287 (2005) 542

[61] C. Derec, A. Ajdari, G. Ducouret, and F. Lequeux, C. R. Acad. Sci. 4 (2000) 1115

[62] R. L. Hoffman, Journal of Colloid and Interface Science 46 (1974) 491

[63] K. Lu and C. Kessler, Journal of Material Science 41 (2006) 5613–5618.

[64] P. D'Haene, J. Mewis, and G. G. Fuller, Journal of Colloid and Interface Science 156 (1993) 350.

[65] F. R. Eirich, Rheology : Theory and Applications, Academic Press Inc., New York, 1960.

[66] A. Kalleder, M. Mennig, and H. Schmidt, Journal of Non-Crystalline Solids 218 (1997) 399

[67] J. Puetz and M. A. Aegerter, Thin Solid Films 516 (2008) 4495

[68] B. Havlinova, L. Hornakova, V. Brezova, Z. Liptakova, J. Kindernay, and V. Jancovica, Colloids and Surfaces A: Physicochemical Engineering Aspects 168 (2000) 251

[69] W. J. Tseng and C.-N. Chen, Journal of Material Science 41 (2006) 1213

[70] J. Koszkul and J. Nabialek, Journal of Materials Processing Technology 157-158 (2004) 183.

[71] F. J. Stadler and H. Munstedt, Journal of Non-Newtonian Fluid Mechanics 151 (2008) 129

[72] M. J. Santtillan, F. Membrives, N. Quaranta, and A. R. Boccaccini, (2008)

[73] E. J. Windhab, in Physicochemical aspects of food processing (S. T. Beckett, ed.), Blacki Academic & Professional, 1995.

[74] L. O. Figura and A. A. Teixeria, in Food Physics : Physical Properties - Measurement and Applications, Springer-Verlang, 2007.

[75] P. G. de Gennes, Reviews of Modern Physics 57 (1985) 827

[76] P. Brocos, Fluid Phase Equilibria 260 (2007) 343

[77] X. Zhang and O. A. Basaran, Journal of Colloid and Interface Science 187 (1996) 166.

[78] P. M. Kosaka, Y. Kawano, and D. F. S. Petri, Journal of Colloid and Interface Science 316 (2007) 671–677.

[79] H. Tavana and A. W. Newman, Advances in Colloid and Interface Science 132 (2007) 1

[80] H. W. Fox and W. A. Zisman, Journal of Colloid and Interface Science 5 (1950) 514

[81] M. Sundberg, A. Mansson, and S. Tagerud, Journal of Colloid and Interface Science 313 (2007) 454

[82] H. Tavana, F. Simon, K. Grundke, D. Y. Kwok, M. L. Hair, and A. Neumann, Journal of Colloid and Interface Science 291 (2005) 497

[83] A. Gosiewska, Journal of Colloid and Interface Science 247 (2002) 107

[84] M. v. Bahr, F. Tigberg, and B. Zhumd, Langmuir 19 (2003) 10109

[85] J. R. Svendsen, Journal of Colloid and Interface Science 316 (2007) 678

[86] T. Papakostas and N. White, Sensor Review 2 (2000) 135

[87] A. Chauvel and G. Lefebvre, in Petrochemical Processes : Technical and Economic Characteristic Imprimerie, Paris, 1989.

[88] D. T. Britton, E. A. Odo, G. G. Gonfa, E. O. Jonah, and M. Harting, Journal of Applied Crystallography 42 (2009) 448.

[89] S. Tanaka, K. B. Min, N. Kato, H. Oikawa, and M. Esashi, IEEJ Transactions on Sensors and Micromachines 125 (2005) 413

[90] M. Wu, Y. Li, D. Wang, and Q. Yin, Ceramics International 34 (2008) 753

[91] J. W. S. Hearle, J. T. Sparrow, and P. M. Cross, The Use of Scanning Electron Microscope, Pergamon Press, Oxford, 1972.

[92] O. D. Solana, in MSc (Physics) Thesis, University of Cape Town, Cape Town, 2009, p. 111.

[93] J. Park and J. Moon, Langmuir 22 (2005) 3506

[94] S.-Y. Kwak, J. Choi, and H. J. Song, Chemical Matter 17 (2005) 1148

[95] S. S. Shenoy and N. J. Wagner, Rheologica Acta 44 (2005) 360

[96] G. Barthelmes, S. E. Pratsinis, and H. Buggisch, Chemical Engineering Science 58 (2003) 2893

[97] D. T. Britton and M. Harting, Pure and Applied Chemistry 78 (2006) 1723.

ACKNOWLEDGEMENTS

First and foremost I would like to thank God for the courage and strength to fulfil my dreams. To my father, Mr. B. Mathe who has through the years has been my pillar of strength and my number one supporter, your faith in me cannot be measured by words.

I could not have done this without the support of my supervisors Prof. M. Härting and Prof. D.T. Britton. I can safely say that my knowledge of science has been greatly enhanced due to your immense support and piercing questions and for that, I thank you. To the CSIR NCNSM and more especially Mr. M. Scriba, thank you for the financial support and for pursuing me to take on this project, your kindness and support through the most trying times of this research was overwhelming.

To my "partners in crime" B. Magunje and W. Solana, those late nights spent in the lab trying to figure out what makes a good ink laid a very solid foundation for our group and I am proud to have worked with you. And to the rest of the UCT Physics Nano group thank you for all your contributions big and small with a special thank you to E. Jonah for his help with curve fitting, you made it an enjoyable exercise. Thank you for answering all my questions with the greatest of ease, you are a true friend. Thank you also to the UCT EMU for help with SEM and optical microscope images.

I cannot forget the love and support of my brothers and sister, friends and both the Mathe and Maloka families who in their own ways made it easy for me to be away from home to pursue my studies, thank you one, thank you all.

This is in remembrance of the two women, mom and grandma, who made me what I am. You may no longer be with us but your love, encouragement and faith in me lives within me every day.